UNIVERSITY OF LEEDS

This is a repository copy of *Stress distribution in reinforced railway structures*.

White Rose Research Online URL for this paper:
https://eprints.whiterose.ac.uk/181961/

Version: Accepted Version

Article:

Esen, AF, Woodward, PK, Laghrouche, O et al. (1 more author) (2022) Stress distribution in reinforced railway structures. Transportation Geotechnics, 32. 100699. ISSN 2214-3912

https://doi.org/10.1016/j.trgeo.2021.100699

© 2021, Elsevier. This manuscript version is made available under the CC-BY-NC-ND 4.0 license http://creativecommons.org/licenses/by-nc-nd/4.0/.

Reuse

This article is distributed under the terms of the Creative Commons Attribution-NonCommercial-NoDerivs (CC BY-NC-ND) licence. This licence only allows you to download this work and share it with others as long as you credit the authors, but you can't change the article in any way or use it commercially. More information and the full terms of the licence here: https://creativecommons.org/licenses/

Takedown

If you consider content in White Rose Research Online to be in breach of UK law, please notify us by emailing eprints@whiterose.ac.uk including the URL of the record and the reason for the withdrawal request.

White Rose university consortium
Universities of Leeds, Sheffield & York

eprints@whiterose.ac.uk
https://eprints.whiterose.ac.uk/

Stress distribution in reinforced railway structures

A.F. Esen[1], P.K. Woodward[2], O. Laghrouche[1], D.P. Connolly[2]

[1]Institute for Infrastructure and Environment, Heriot-Watt University, Edinburgh EH14 4AS, UK

{afe1, o.laghrouche}@hw.ac.uk

[2]Institute for High-Speed Rail and System Integration, University of Leeds, Leeds LS2 9JT, UK

{p.k.woodward, d.connolly}@leeds.ac.uk

Abstract

This paper evaluates the performance of a geosynthetic reinforced soil retaining wall (GRS-RW) system as an alternative to a conventional railway embankment. The aim is to investigate the behaviour of the GRS-RW system in terms of displacements and stress levels at different locations in the track and substructure. Full-scale laboratory experimental testing is carried out on a GRS-RW structure, supporting sections of ballasted and slab track, under moving loads at 360km/h. The tracks are supported by a low-level fully confined conventional embankment and a GRS-RW system, which are constructed to high-speed standards. Displacement transducers and earth pressure cells are placed at different locations to record the displacements of the track and the stress levels in the substructure. The test results show that the pressure levels on the GRS-RW wall are negligibly small for the particular test setup, proving the GRS structure under the action of compaction reached its active state. This means that the reinforced soil was self-supporting under its self-weight and train loads, meaning there was minimal pressure on the walls. Therefore, GRS-RW systems are better alternatives to traditional earth embankments due to enhanced soil stabilisation and less land take.

Keywords: Full-scale railway track testing; railroad ballasted track; high-speed rail slab track; conventional embankment; Geosynthetic Reinforced Soil; high-speed railway earthworks

1 Introduction

One of the most important purposes of railway track beds is to transfer the load adequately to the formation below the track. The magnitudes and distribution of pressure exerted by heavy axle load significantly influence the short- and long-term behaviour of railway tracks. The induced stresses on the subgrade can be influenced by axle load, formation thickness, sleeper spacing, rail bending stiffness, and presence of any additional layer for load distribution. Lowering the groundwater table, stabilizing the subgrade and introducing geosynthetics can improve the threshold stress of subgrade soil [1]. Geogrids have been shown to be a practical solution when placed in ballast [2, 3, 4] and soil [5, 6, 7, 8, 9, 10, 11] to reduce plastic settlement and improve stress distribution. Geogrids also proved to increase the overall stability of the railway tracks via preventing particle translations and providing better drainage behaviour [12]. A thorough understanding of the pressure distribution from top layers to formation is required to design railway tracks satisfactorily, preventing substantial and frequent maintenance. For this purpose, numerous field and laboratory tests were performed to identify stress behaviour at certain depths under various axle loads and speeds. However, measuring pressure can be difficult in laboratory conditions, for example, Brown *et al*. [13] incorporated pressure cells under the ballast in a full-scale testing facility and collected the transient vertical stresses at the top of the subgrade, which varied greatly at the early stages of the testing.

Liu & Xiao [14] presented two field data sets also collected in China for a passenger carrier travelling at 200km/h with 14t axle load and another one corresponding to a freight train with 22.5t axles travelling at 120km/h. The stress pulse waves on the subgrade were recorded. Two test sites were investigated by Anderson & Rose [15] with the focus on the presence of an asphalt layer. The pressure distributions and rail deflections were obtained by using earth pressure cells and displacement transducers at critical interfaces. Interfacial pressure measurements were recorded in the field by Rose *et al.* [16] presenting the pressure levels in the ballast and displacement magnitudes in a six-consecutive-sleeper section over several month-long heavy freight train passage procedure. It was found out that the pressure distribution is highly dependent on the compaction level of the ballast, however, disregarding the measurements from non-uniformly compacted ballast, the peak pressure at the sleeper-ballast interface was identified. In-situ tests were performed to obtain the pressure measurements at the interfaces of rail base-sleeper, sleeper-ballast, ballast-subballast and subballast-subgrade by Rose *et al* [17]. The peak pressure on the conventional and hot mixed asphalt trackbeds subjected to 36 tonnes-axle was recorded. Field tests were conducted in Australia by Indraratna*et al* [18] to investigate the reduction in the vertical stresses along with the depth. The vertical stresses caused by two types of trains with different axle loads, one of which has wheel irregularities, traversing a track section confined with geosynthetics were recorded. More field data on various tracks were recorded by Cardona *et al.* [19]. Field measurements of the dynamic stress in the subgrade surface was 13-20kPa in the case of slab track and it ranged between 50-100 kPa for the ballasted track's case [20, 21, 22, 23, 24]. Evidently, the dynamic stresses in the subgrade under a slab track were 4-5 times less than those under a ballasted track. The stresses in the soil increased with the increase in the train speeds.

A direct relation between track modulus and stresses induced in the subgrade in the presence of heavy axle loads was presented by Li [25] using the Facility for Accelerated Service Testing (FAST). The term track modulus is described by Li [25] as *”Track modulus is a parameter defined by a model of the beam (rail) on elastic foundation, and is used extensively to quantify the track foundation support or the overall stiffness of ballast, subballast and subgrade layers”*, based on Selig and Li [26]. A full-scale test of an asphalt railway track was carried out by Yu *et al.* [27] to find out the stresses in the subgrade. Three pressure cells were incorporated under a three-sleeper section track on the ballast foundation, and pressure change and permanent sleeper and subgrade settlements during 350 MGT cyclic loading were recorded. Jiang *et al.* [28] and Chen *et al.* [29] and Zhang *et al.* [30] carried out full-scale laboratory tests of ballastless track. The stresses were recorded at different depths of the subgrade. Lee *et al.* [31] performed full-scale tests on three combinations of ballastless track with asphalt trackbed to investigate the most effective stress distribution. A small-scaled box test was performed by Sysyn *et al.* [32] to determine the stress distribution immediately underneath the ballast. The cyclic load was applied on a sleeper position in a 1m x 0.17m x 0.33m box filled with crushed stones. A total of 11 loading sensors were positioned under the stones along the sleeper to investigate the stress distribution caused by a single sleeper. Rose *et al.* [33] performed a series of laboratory tests using earth and granular materials pressure cells to estimate the vertical pressure levels between a sleeper and ballast. Cyclic triaxial tests were carried out to study the performance of railway components under repeated loading [34, 35]. True triaxial tests with controlled confined stresses and vertical stress were also performed by Yu *et al.* [36] and Yu *et al.* [2]b to identify the resilient behaviour of ballast and subballast. Liu & Xiao [14] carried out cyclic triaxial tests for compacted silt specimens combined with field measurements of subgrade stress to study dynamic stress-bearing of subgrade. Momoya *et al.* [37] and Ishikawa *et al.* [38] performed cyclic and dynamic tests over a 1:5 scaled 15-sleeper long model experimentally. The laboratory findings were used to calibrate a three-dimensional linear finite element model and to compare vertical stress distribution in the subgrade of different types of tracks. Bian *et al.* [39] also performed full-scale testing on a ballastless track under three different train speeds. The findings were used by Bian *et al.* [40] to study the geodynamic issues in high-speed railways using a 3D dynamic FEM model. It was commonly evident that slab tracks transfer the loads more uniformly to bottom layers than ballasted tracks.

A 2D dynamic finite element analysis was performed by Yang *et al.* [41] to identify the stress state of the ground and the stress path during loading by the trains at different speeds and Powrie *et al.* [42] investigated the stress state of the soil and elastic parameters using 2D and

3D FEM models. Their models, validated over the field data obtained by Grabe *et al.* [43], investigated the static and dynamic behaviour of the soil based on the ratio of train and Rayleigh wave speed. As long as the train speed does not exceed 10% of Rayleigh wave speed, the track behaves in a quasi-static manner. However, the stresses can be underestimated by 30% when the train speed reaches 50% of Rayleigh wave speed. Cardona *et al.* [44] developed a 2D model of three different tracks with and without bituminous layers, and validated against the stress measurements collected at the French Est-European HSL under the passage of TGV at 317km/h of which details were presented by Cardona *et al.* [45]. The effect of cracked sleepers on stresses between each layer of the substructure was studied by Domingo *et al.* [46] using a 3D finite element model, which was validated with real track data. Shahu & Kameswararao [1] also created a 3D model to assess the induced stresses in the subgrade surface and approximate acceptable ranges of resilient moduli for sub-layers and formation thickness, comparing against design parameters proposed by ORE [47]. Jiang *et al.* [28] studied the stresses at four different depths of the subgrade under ballastless track using a 3D dynamic model. Shan *et al.* [48] investigated vertical dynamic stress of the subgrade surface at transition zones using a 3D model which was validated with field measurements. Dong *et al.* [49, 50] created a model using a thin-layer finite element capable of computing the dynamic stresses and strains. Ramos *et al.* [51] developed a 3D model adapted to ballasted and slab tracks which were calibrated with full-scale laboratory tests to investigate the stress path in soil under cyclic loading. Bathurst & Kerr [52] proposed an analytical model to predict the vertical stresses utilizing the Boussinesq theory and beam on elastic foundation method. Fadum [53] proposed a chart to identify the influence factors for the vertical stress beneath the corners of a rectangular foundation. The chart is used to compare the laboratory results obtained in this research.

The full-scale laboratory tests presented in this study were performed in Geopavement and Railways Accelerated Testing Facility (GRAFT-2). In this paper, the purpose is to compare stress levels in the soil under concrete-slab and ballasted tracks on a conventional embankment [54] with a low-level wall simulating the remainder of the slope and under a Geosynthetically Reinforced Soil with Retaining Walls (GRS-RW) structure [55]. The stress levels at various depths under static and cyclic loading were experimentally investigated. In addition to the comparison of the experimental results obtained in this research, field and experimental data presented by various authors were used for further comparison. The main limitation of this research work was the confinement of the testing box, in comparison to real field conditions. However, the presented experimental testing is used for the sake of comparison of different configurations under exactly the same conditions.

This paper is organised as follows; The testing facility, experimental setup and data acquisition are described in Section 2. The static and cyclic loading methodology is presented in Section 3 and the analysis of the results and comparison against the literature are discussed in Section 4. The main concluding remarks and ideas for future work are presented in Section 5.

2 Laboratory testing

In this laboratory-based experimental research work, two types of substructures were investigated. The first substructure was constructed based on conventional embankment parameters and the second substructure concerns the GRS-RW structure [54, 55]. Both structures were built using the same sand properties and moisture content. The compaction pattern of the sand on each structure was the same. The soil consisted of two layers which are the subgrade and frost protection layer (FPL). The superstructures used in this research are a slab track and a ballasted track. The slab track consisted of the hydraulically bonded layer (HBL), grout and precast concrete slab. The ballasted track had railway ballast, triangular aperture shaped geogrid under the ballast bed and concrete sleepers.

The substructure was composed of well-compacted 0-6mm graded limestone sand mixture, which was chosen from two different batches composed of 0-6mm well-graded granular limestone. The sand was composed of 80% of 0-4mm batch and 20% of 2-6mm batch (***Figure 1(a)***). The uniformity coefficient (Cu) and the coefficient of gradation (Cc) of the sand was 11 and 1.604, respectively. The optimum moisture content, which is 5% as seen in ***Figure 1(b)***, was determined by modified proctor compaction tests. A higher optimum moisture content, which is 7%, was identified with the standard proctor test but the modified proctor test results were more suitable for the given substructure because a heavy compaction method was used while constructing it. A 140kg diesel forward/reverse plate compactor with 25kN compaction force vibrating at 90Hz was used. The compaction tests were carried out following the procedures stated in BS 1377-4-1990 [56]. The maximum dry density was identified as 22.2kN/m^3. The subgrade was compacted using two passes and the FPL using four passes, with each pass consisting of forward and reverse compaction.

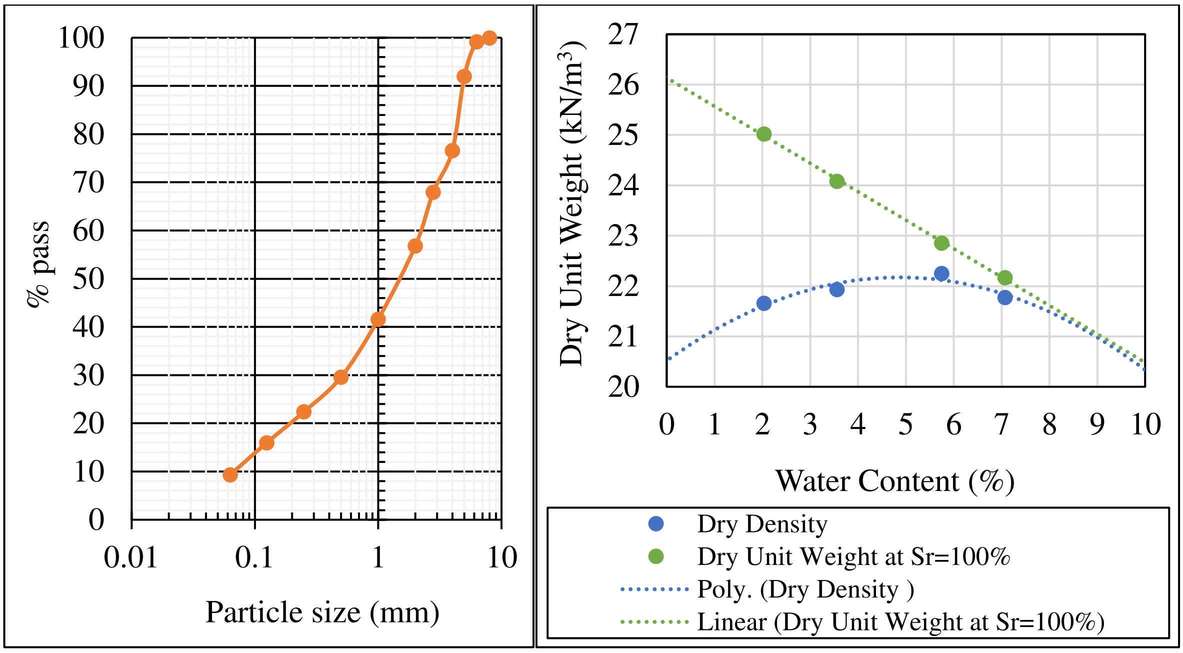

(a) ***(b)***

Figure 1: (a) Gradation curve of the sand (b) Compaction curve The structural characteristics of unbound materials in railway substructures and road pavements were determined using the Transport and Road Research Laboratory (TRRL) dynamic cone penetrometer (DCP). DCP readings were recorded in the GRAFT-II facility at six different locations after each compaction stage. A correlation between DCP reading and CBR was linked through log10(CBR)=2.48-1.057×log10(mm/blow) proposed in reference [57]. The deflection modulus E_{v2} was verified using a static plate load test in accordance with DIN-18134 standard [58]. In this paper, the E_{v2} value of the FPL was estimated through the plate load test to be 133.55mN/m^2 and the E_{v2} value of the subgrade to be 67.71mN/m^2. The Young's modulus of the compacted sand was calculated based on the DCP and PLT tests' results using $E_{dyn} = 2 \times E_{v2} = 100 \times CBR[\%]$ derived in the reference [59]. More details about sand gradation curve and compaction method were described in detail in references [54] and [55].

2.1 Experimental setup

Full-scale laboratory-based testing was used to compare the static and cyclic performance of a precast concrete slab track section to a ballasted track (with concrete sleepers) resting on a compacted substructure. The railway track substructure was constructed from a 1.2-metre-deep compacted soil, comprised of subgrade and FPL, according to modern high-speed rail standards. ***Figure 2*** shows the testing facility and the tracks tested.

(a) ***(b)*** ***(c)*** ***(d)***

Figure 2: ***(a)*** *The slab track on the embankment -ES-,* ***(b)*** *the ballasted track on the embankment -EB-, **(c)** the slab track on GRS-RW system -GS-,* ***(d)*** *the ballasted track on GRS-RW system -GB-*

The conventional embankment had a low-level wall to simulate the remainder of the slope and it was fully connected to the rig so it cannot move. This was considered to represent the slightly enhanced embankment and was used because of the confines of the testing facility. The soil was formed of 800 mm deep subgrade and 400 mm deep FPL. The embankment constructed in GRAFT-2 was fully confined, from the four sides [54]. Dynamic cone penetrometer (DCP) and plate load test (PLT) were performed to identify California bearing ratio (CBR) and the second deformation modulus (E_{v2}), respectively, in the subgrade and FPL as shown in ***Table 1***. The top soil layer is called FPL in the ballasted track also to be consistent with the description used in the slab track case.

Table 1: CBR values of the compacted soil using Dynamic Cone Penetrometer (DCP) and E_{v2} values collected by Plate Load Testing (PLT)

CBR Test Time	***Conventional Embankment CBR***	***GRS-RW CBR***	***E_{v2} (MPa)***
During construction of Substructure -Subgrade	31.76	28.5	67.71
During construction of Substructure -FPL	43.36	56.1	133.35
After Removal of Slab - on top of FPL	120.56	125.1	-
After Removal of Ballast – on top of FPL	120.56	128.2	-

The second tested type of substructure was the GRS-RW structure [55]. This substructure consisted of 0.1m well-compacted base layer on top of which the 1.2m thick GRS-RW was built. The concept of the GRS-RW structure was inspired by [60, 6, 8]. The substructure was constructed with compacted soil and sandbags which were hand wrapped and reinforced with RE540 (Tensar) uniaxial geogrids. The purpose of the sandbags was to provide a supportive wall to soil while wrapping it with geogrids and to facilitate the drainage. The average aperture size of the geogrid is 16mm x 219 mm with 64.5kN/m short term tensile strength in longitudinal direction [55]. The GRS-RW structure was confined by the retaining walls in the track direction, as well as the GRAFT-2 walls in the lateral direction and was anchored with tie bars with angle irons positioned in the soil (**Figure 6**). A retaining wall was made of a thick steel plate positioned 0.08m distance from the sandbag wall. The gap between the steel plate and the sandbags was then filled with a ready-mix highly fluid self-compacting concrete called topflow. However, as the retaining walls were only anchored to the compacted sand, they were free to move laterally under the anchored system. Therefore, the full confinement for GRS-RW was solely in the longitudinal direction, whereas in the conventional embankment test the substructure was confined in both longitudinal and lateral directions by the walls of GRAFT-2.

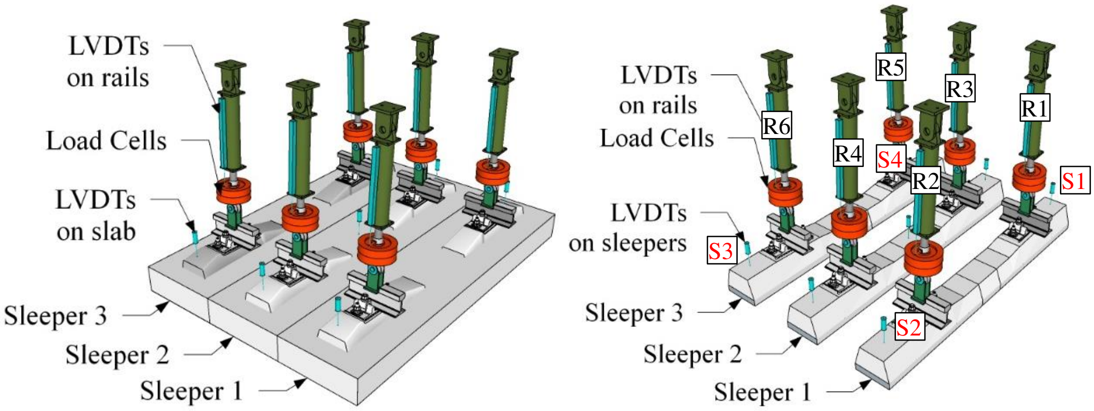

(a) ***(b)***

Figure 3: *LVDT positions and labels (a) slab track (b) ballasted track*

The first tested form of the superstructure was a precast reinforced concrete slab track manufactured by Max Bögl (***Figure 2(a)***). The hydraulically bonded layer (HBL) layer, made of C10/12 concrete with characteristic cube compressive strength of 10 MPa, which is a lightweight and low strength concrete. The HBL was cast on the compacted soil with a thickness of 300mm. The slab track was positioned above the HBL after 21 days and a highly fluid cementitious grout was poured to form the 30-40mm thick binding layer with the HBL. The second tested superstructure form was a ballasted track. The three standard G44 reinforced concrete sleepers were embedded in the ballast bed, which was laid and compacted in four equal layers of 100mm each, hence the thickness of the ballast underneath the sleepers was 400mm. The ballast was supported by a triangle-aperture geogrid TX190L. The same railpads were used on both the G44 sleepers and the slab track.

The first considered test concerned the slab track on the conventional embankment (***Figure 1(a)***). After completion of the slab track tests, all slab track components (HBL, grout and the slab) were removed from the testing rig. The surface of the soil was treated as the cast-in HBL disturbed the top layer. Then the ballasted track was placed on the conventional embankment (***Figure 1(b)***). After completing the test, the ballasted track was removed, and the substructure was excavated from the GRAFT-2 rig to prepare the testing of the slab track on GRS-RW (***Figure 1(c)***) and then followed by the ballasted track on GRS-RW (***Figure 1(d)***). The same testing procedure was followed, and the same material properties were used for all four tests.

2.2 Data acquisition

Displacement transducers and earth pressure cells were employed to determine the displacements and stresses under static and cyclic loading. There were 6 channels for load cells, 6 channels for the displacements of the rails, 7 channels for the displacements of the sleepers/slab and 5 channels for pressure cells actively used to acquire data. The sampling rate of the data acquisition system was 200Hz per channel.

The displacement transducers' locations are shown in ***Figure 3***. The LVDT choice was crucial for these tests as both deflection, which is the instantaneous/transient displacement, and settlement, which is the irrecoverable deformation under millions of cycles, must be acquired. Therefore, the LVDTs needed to be sensitive enough to record the sinusoidal motion of the slab, which can be as small as a hundredth of a millimetre, as well as the accumulated settlement of the sleepers in the ballast after 3.4 million cycles, which was greater than 10 millimetres [55].

The model 3510 earth and the 3515 granular materials pressure cells were used to measure vertical stresses. These semiconductor type pressure cells had 9-inch diameter plate which is capable of measuring up to 1MPa with 0.015kPa sensitivity. The pressure cells were incorporated at different locations in the conventional embankment. In this case, one earth pressure cell was placed in the subgrade (SG-PC) and another one in the FPL (FPL-PC) directly under the central sleeper. The three granular material pressure cells were placed at the top of FPL; two under the rails and one under the midpoint of central sleeper (denoted as track pressure cells; T-PC1, T-PC2, and T-PC3), as shown in **Figure 4**.

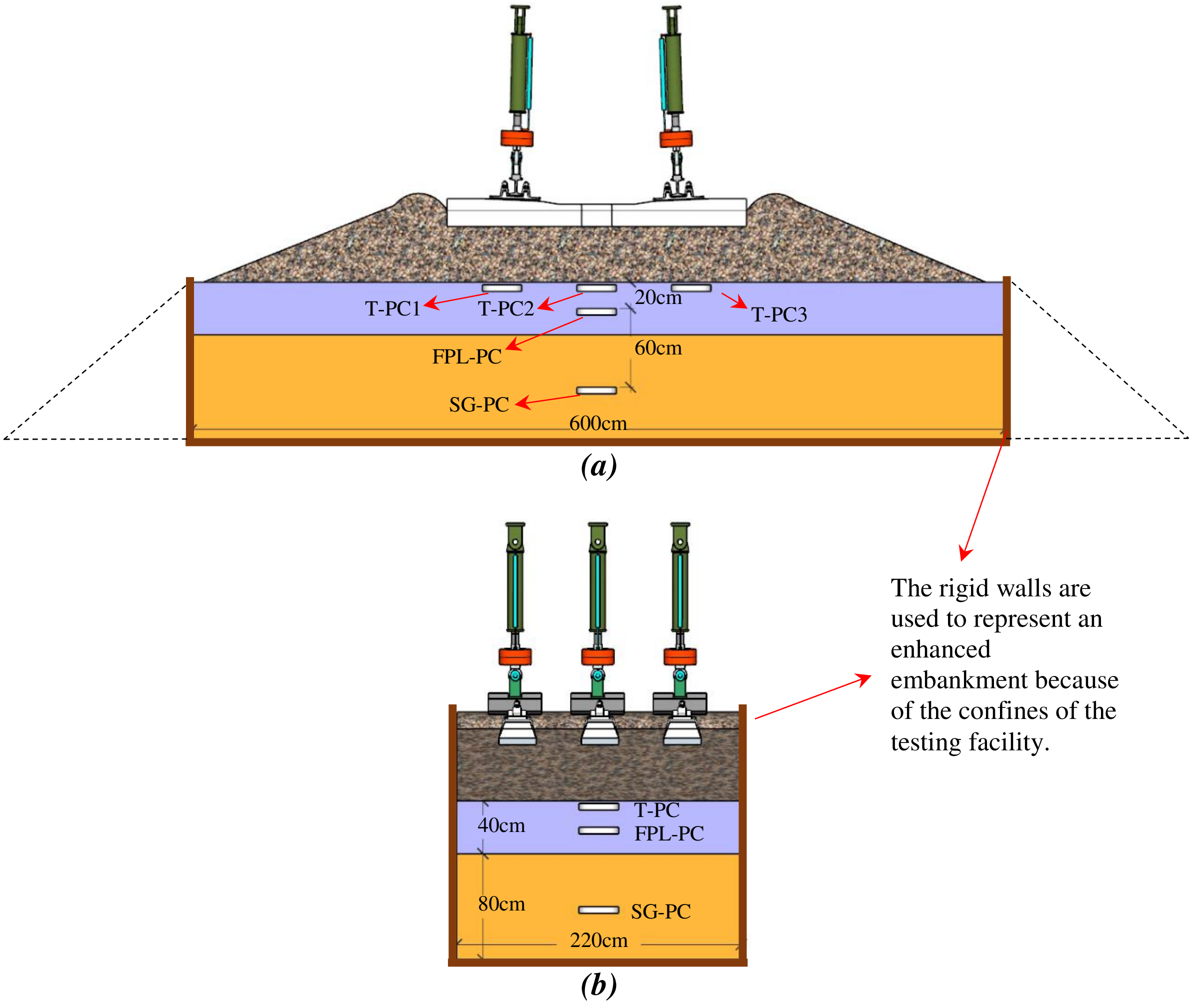

Figure 4: The positions of the pressure cells in the conventional embankment (a) Lateral cross-section of centre (b)Longitudinal cross-section of the centre

As the same pressure cells used for both slab track and ballasted track cases, the T-PC pressure cells were embedded in the soil, 50mm below the interface of the HBL and FPL, and ballast and FPL, respectively, and then covered with compacted soil (***Figure 5(a)***). A spirit level was used while installing the pressure cells so that they provide measurements of vertical stresses (***Figure 5(b)***).

(a) *(b)*

Figure 5: The installation of pressure cells in the soil (a) The T-PC pressure cells near the surface of FPL (b) Levelling a pressure cell

The GRS-RW structure on the other hand had two earth pressure cells incorporated in the soil. The SG-PC and FPL-PC were placed exactly in the same location as in the case of conventional embankment, as indicated in **Figure 6**. While T-PC pressure cells were positioned below the ballast, the same pressure cells were positioned in the inner side of the retaining walls to measure the pressures exerted on the walls in the GRS-RW case and denoted as W-PC.

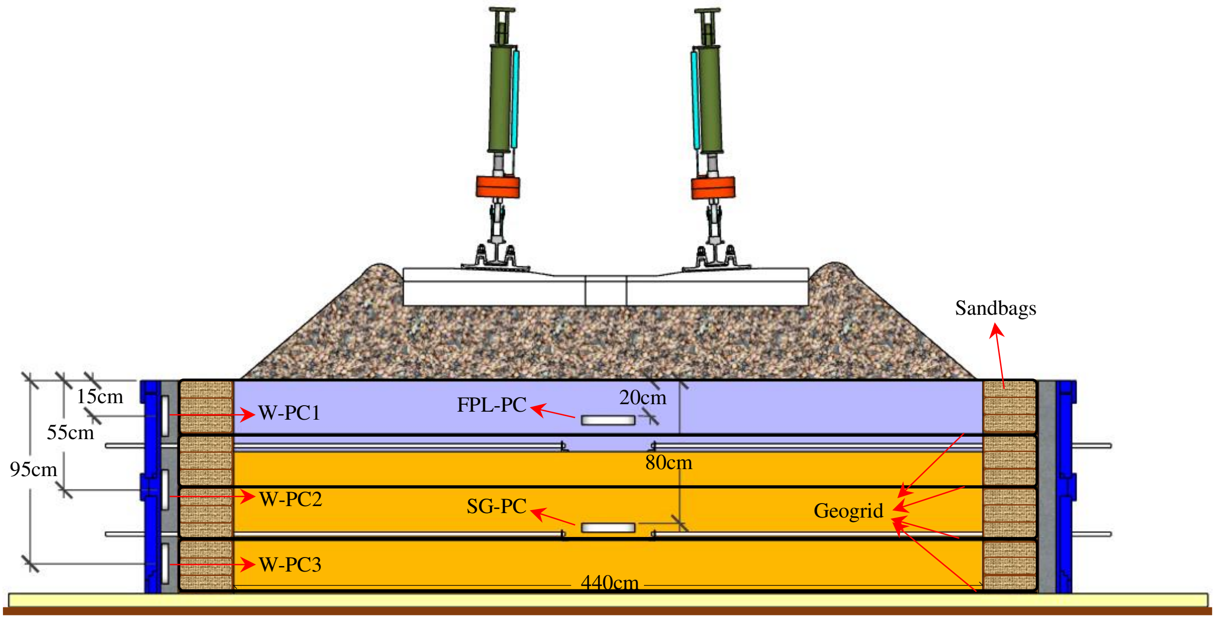

Figure 6: The positions of the pressure cells in the GRS-RW structure

The pressure cells on the wall were labelled as W-PC (***Figure 7(a)***). After attaching the pressure cells, the wall was positioned 8-10cm away from the sandbag wall (***Figure 7(b)***). This gap was then filled with "topflow", which is a ready-mix highly fluid self-compacting concrete consisting of 10 mm diameter aggregates (***Figure 7(c)***). This material was chosen specifically because of its ability to fill the gaps between the geogrid and the sandbags through the geogrid apertures. This was intended to provide reinforcement and resilience to the GRS. The purpose of the W-PC pressure cells was to obtain the pressure levels due to the lateral expansion of the GRS structure.

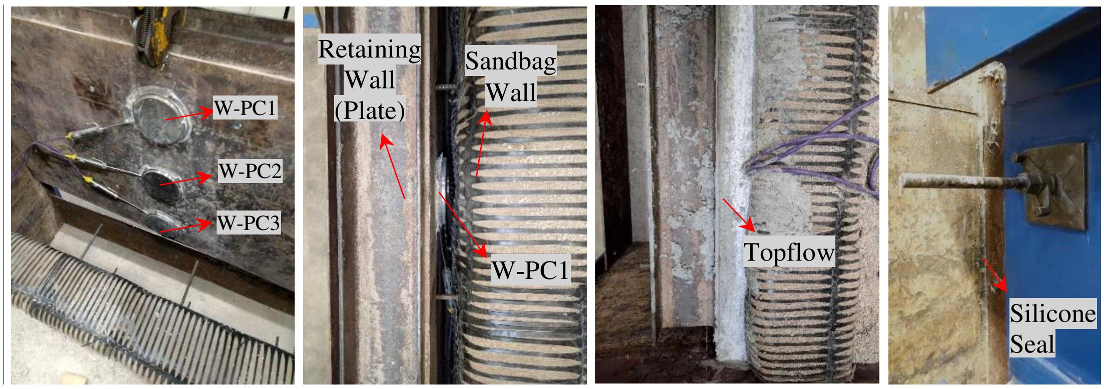

(a) *(b)* *(c)* *(d)*

Figure 7: W-PC pressure cells (a) on the retaining wall (c) Gap filling material topflow (d) Silicone sealant on the sides of the wall to prevent leakage

3 Testing methodology

In this study, two static tests and two cyclic tests were performed. In the static tests, first, a 13-tonne axle load (Static I) with load redistribution was applied on the track for approximately 10 minutes and then the load was increased to simulate a 17-tonne axle load (Static II) for the same length of time (**Table 2**). While half of the axle load was applied on the middle sleeper, one quarter axle load was applied on each neighbouring sleeper. In this way, 100% of the axle load was distributed over the three-sleeper track section during static loading. This distribution approach was derived from the beam-on-elastic-foundation theory. The load was distributed on three separate rail segments. The load distribution can be recalculated according to the number of sleepers and, therefore, the displacement will change. The displacement will reduce if the number of sleepers increases.

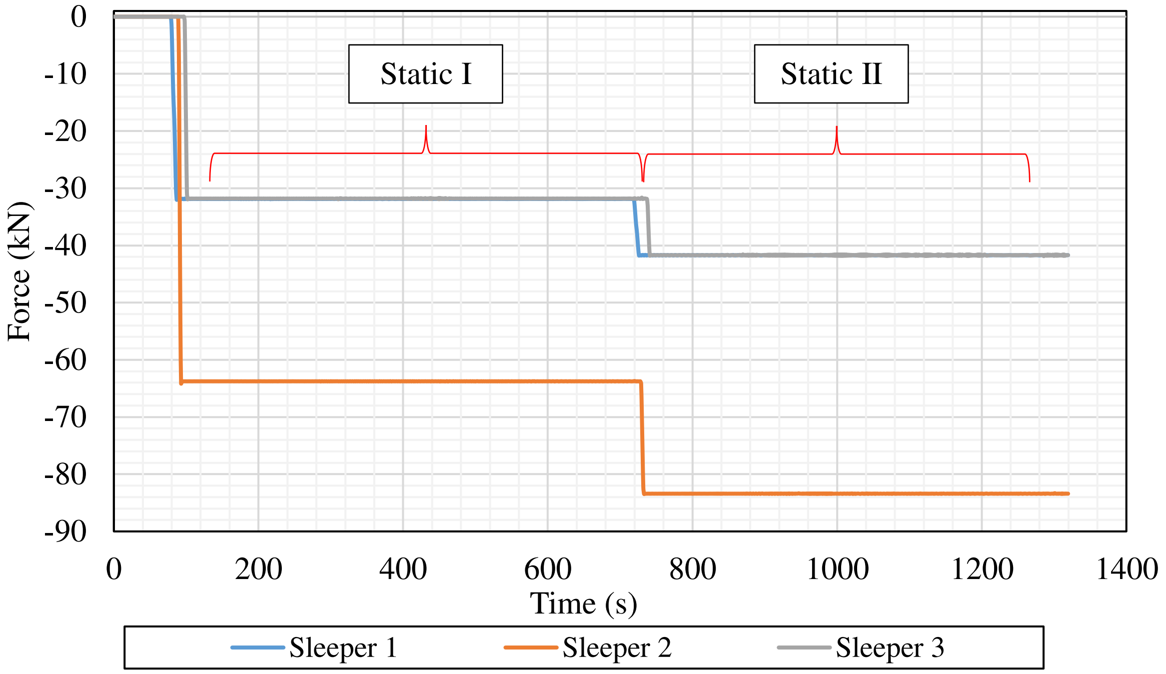

Figure 8: Distribution of axle loads over three sleepers

The orange line in **Figure 8** represents half of the axle load on the middle sleeper (Sleeper 2) while grey and blue lines represent a quarter of the axle load on the adjacent sleepers (Sleeper 1 and Sleeper 3). The magnitudes of the loads are indicated in **Table 2**.

Table 2: Loading sequence of the ballasted and concrete slab track tests

Test	***Static I***			***Static II***			***Cyclic I***			***Cyclic II***		
Axle Load (t)	13			17			13			17		
Duration	600s			600s			1.17×10^6 cycles			2.20×10^6 cycles		
Frequency (Hz)	N/A			N/A			5.6			2.5		
Δt - Time Interval (s)	N/A			N/A			0.0065			0.0065		
Load per sleeper (%)	25	50	25	25	50	25	100	100	100	100	100	100
Load per actuator (kN)	15.94	31.88	15.94	20.84	41.69	20.84	58.9	58.9	58.9	83.4	83.4	83.4
Load per Sleeper (kN)	31.88	63.76	31.88	41.68	83.38	41.68	117.8	117.8	117.8	166.8	166.8	166.8
	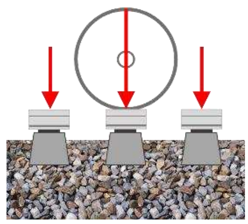			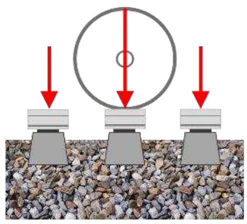			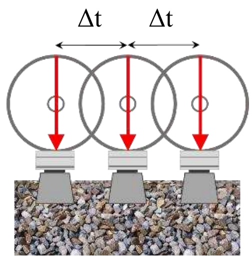			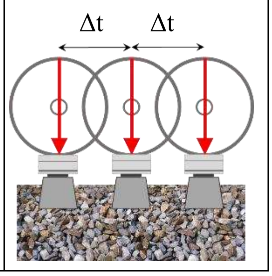		

After the static tests, cyclic loading began without any load redistribution, by applying 13-tonne axle load and then 17-tonne axle load on each sleeper with a time phase lag, as indicated in Table 2. This approach was implemented in both cyclic loading tests to simulate the worst-case scenario and to allow direct comparisons of settlement behaviour between different track types and substructure forms, for the same cyclic loading condition. The sleepers were therefore subjected to repeated loads to simulate moving axles at 360km/h at a set frequency. The phased nature of the loading allows for principal stress rotation effects to be simulated and ***Figure 9*** shows a typical phase/time lag between the sleepers; this phasing mimics the axle moving from one sleeper to the adjacent one in 0.0065 seconds, which is illustrated in ***Table 2*** as Δt. The cyclic tests were performed at 2 different frequencies: 1.17 million cycles at 5.6Hz and 2.2 million cycles at 2.5Hz. The load applied at 5.6Hz was oscillating between 13kN and 58.9kN -Cyclic I- per actuator, giving 117.8kN per sleeper, and the load at 2.5Hz was oscillating between 5kN and 83.4kN -Cyclic II- per actuator, giving 166.8kN on each sleeper (***Figure 9***).

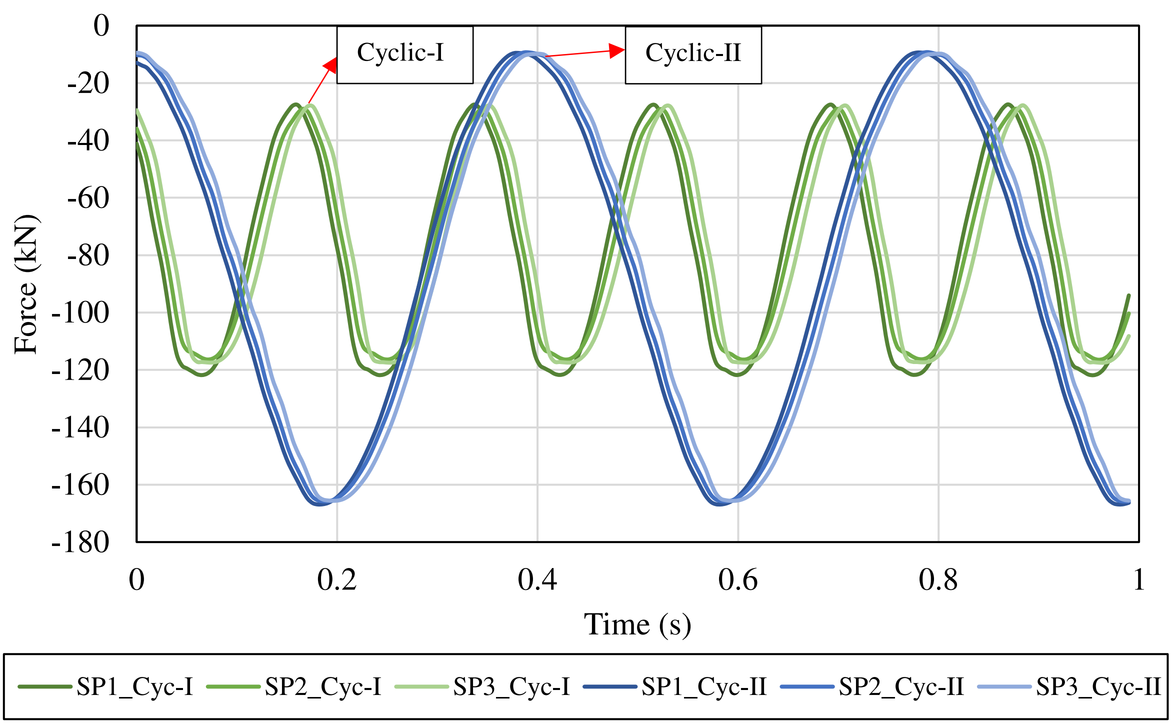

Figure 9: Time interval of sequential actuator loading of cyclic loads in a second on each sleeper

4 Analysis

In this section, results related to the static and cyclic loading tests are presented and analysed. ***Table 3:*** summarizes the notations and abbreviations used for the classification of the data. Different colours and shades are also used for convenience and clarity of the figures in the analysis section.

Table 3: Abbreviations of the track types and sensors

Substructure	***Embankment***		***GRS-RW***	
Superstructure	Slab	Ballasted	Slab	Ballasted
Notation	ES	EB	GS	GB
Pressure Cells in the subgrade	SG-PC			
Pressure Cells in the FPL	FPL-PC			
Pressure Cells under the Track	T-PC1 T-PC2 T-PC3		N/A	
Pressure Cells on the wall	N/A		W-PC1 W-PC2 W-PC3	
Displacements Transducers on Rail	R			
Displacements Transducers on Sleepers	S			

4.1 Static loading

An initial static distributed axle load was applied on the considered tracks. First, 13t (127.54kN) -Static I- and then 17t (166.76kN) -Static II- were applied for approximately 10 minutes each. The distribution of these axle loads, over the three-sleeper area, is described in ***Figure 8***. The analysis of displacements of the rails and the sleepers/slab, as well as the stresses in the soil, are presented.

4.1.1 Displacements

Figure 10 illustrates the averaged displacements of rails on sleeper 1 and sleeper 3, which were subject to a quarter of the axle load. The average of the four displacement transducers positioned at the corners of the track was taken into account to plot the displacement curve for each track. It is evident that the rail displacement on sleepers 1 and 3 of the slab track on the conventional embankment (ES) is 13% lower than that of the slab track on GRS-RW structure (GS). The rails on ballasted track on GRS-RW structure (GB) deflected 35% more than in the case of the conventional embankment (EB). Half of the axle load was applied on sleeper 2 (middle sleeper) for which the displacements of the rails are shown in ***Figure 11***. The central rails on EB and GB tracks deflected twice as much as the rails on slab on both ES and GS tracks. However, the conventional embankment and GRS-RW structure performed in a very similar way. Additionally, as it can be seen from the comparison of ***Figure 10*** and ***Figure 11***, the rail displacement of sleeper 2 is nearly double of the displacement of the sleepers 1 and 3, for all four tracks.

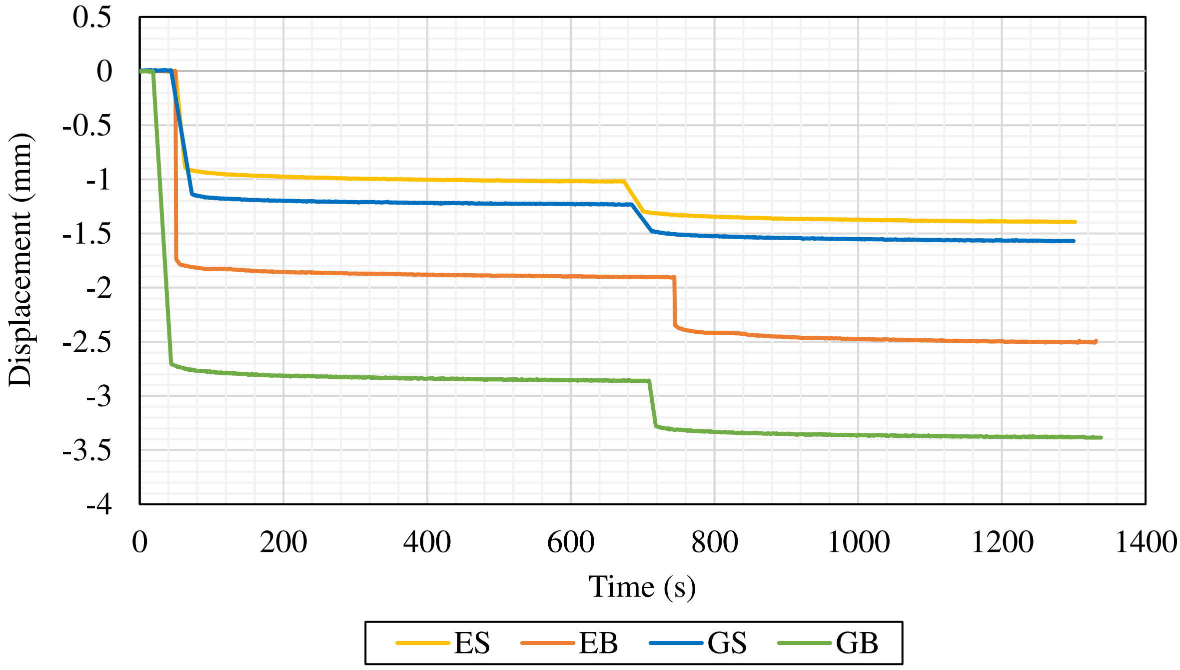

Figure 10: Average vertical displacement of the rails on sleeper 1 and 3 under static loading

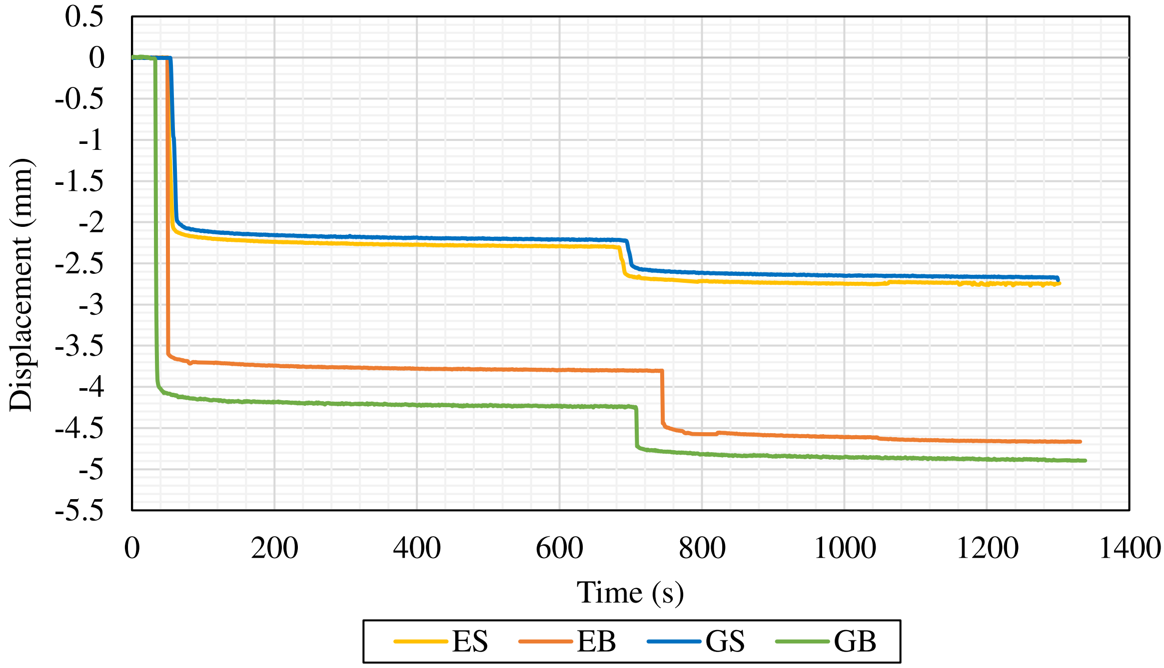

Figure 11: Average vertical displacement of the rails on sleeper 2 (middle sleeper) under static loading

The displacements recorded at the corners of the concrete slab-track and the ballasted track (Sleeper 1 and Sleeper 3) are shown in ***Figure 12***, and the displacement of the middle sleeper is shown in ***Figure 13***. The corners of the slab track deflected the similar amount, which is 0.03-0.04mm in ES and 0.06mm-0.07mm in GS, proving a more uniform load distribution. On the other hand, the Sleeper 1 and Sleeper 3 deflected significantly less than Sleeper 2 in both EB and GB cases. Although the rails deflected linearly depending on the magnitude of the load, the sleepers in the ballasted tracks deflected unevenly due to the highly non-uniform and unbound nature of the ballast. Additionally, the sleepers 1 and 3 in ES deflected 35 times less than in the case of EB, and for GS it is 12 times less than for GB. In the case of Sleeper 2, ES and GS deflected 33 and 35 times less than in the cases of EB and GB, respectively.

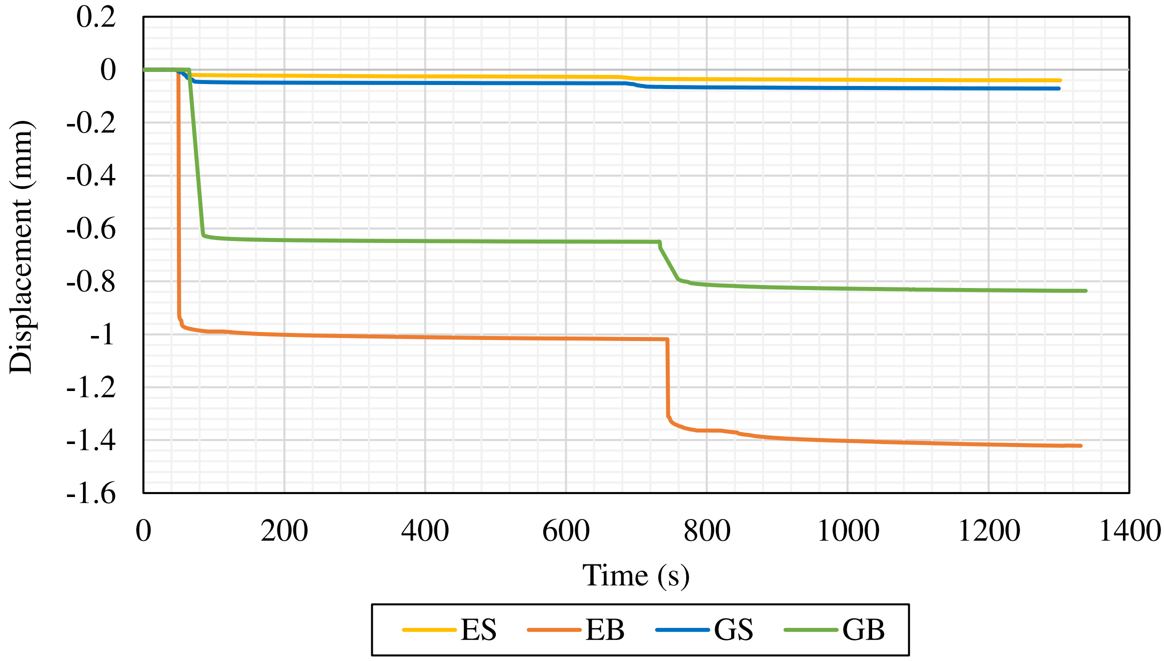

Figure 12: Average vertical displacement of sleeper 1 and 3 under static loading

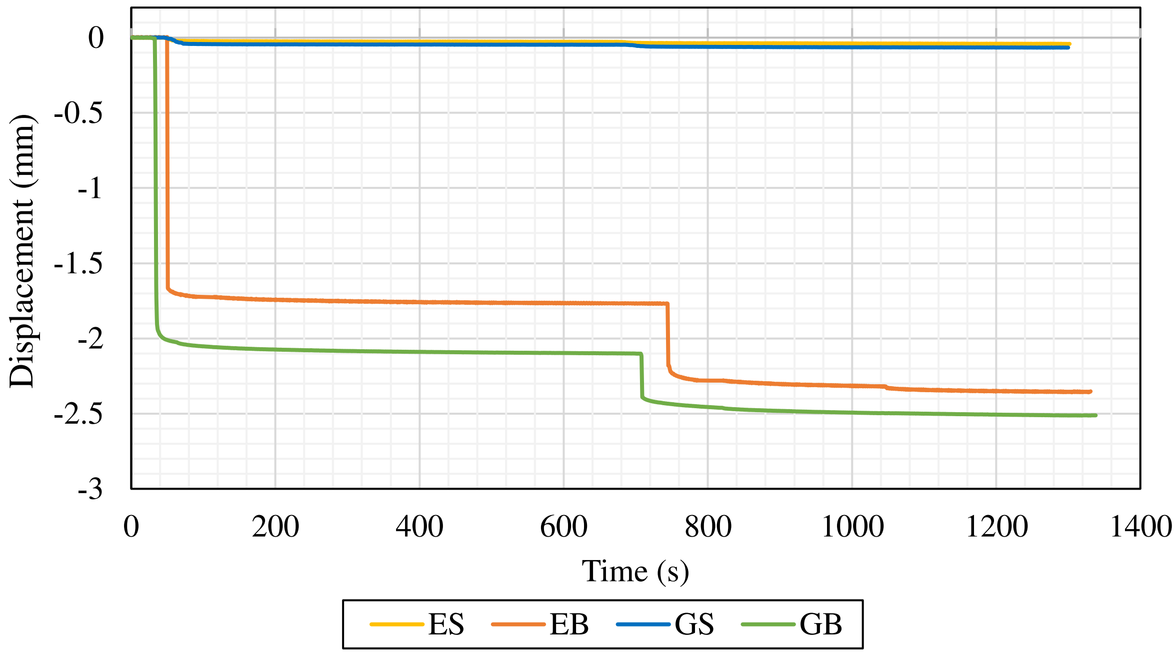

Figure 13: Average vertical displacement of sleeper 2 (middle sleeper) under static loading

4.1.2 Stresses

The stresses immediately under the slab and the ballasted track on the conventional embankment under Static-I and Static-II loading are illustrated in ***Figure 14***. The exact positions of the pressure cells (T-PC) were shown in ***Figure 4***. The stress levels under the rails in the slab track were approximately double the stress level in the centre of the track, whereas, in the ballasted track, the stress under one rail was 25% less than the records taken at the other three pressure cells proving the non-uniformity of the ballast under the sleeper despite the presence of the ballast geogrid. The average stress measured under the HBL was 50% less than the stress under the ballast. The rise in the stress level when the load increased from 13t to 17t was linear in both tracks, slab and ballasted, which lead to 1.3 times higher stresses, as expected. The pressure distribution in the ballasted track can vary depending on the initial ballast condition and compaction.

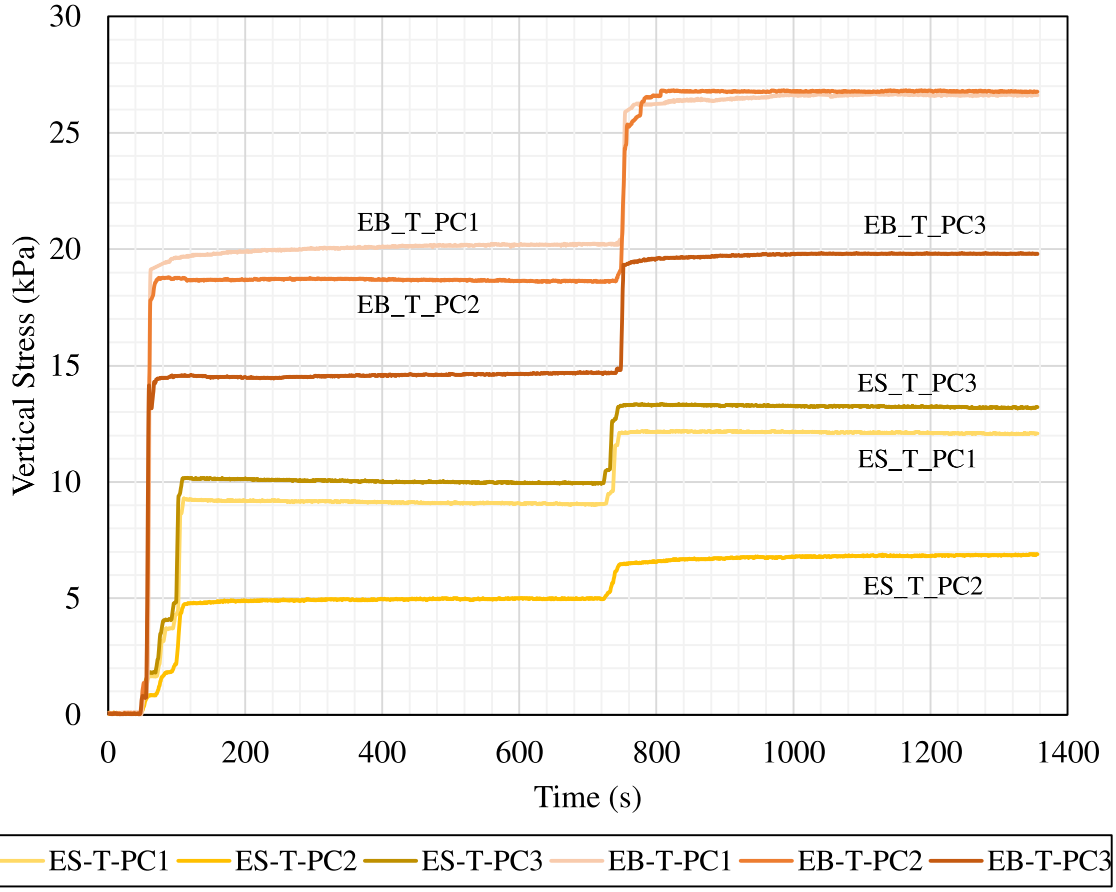

Figure 14: Vertical stresses immediately under the slab (ES) and the ballast (EB) tracks on the conventional embankment under static loading

Figure 15 and ***Figure 16*** illustrate the stresses in the centre of the subgrade and FPL, which are 80cm and 20cm below the FPL surface, respectively, as shown in ***Figure 4*** for the conventional embankment and ***Figure 6*** for the GRS-RW structure. The stress levels decreased along with depth closing the stress gap between tracks e.g. ES-FPL was 3 times smaller than EB-FPL but ES-SG was similar to EB-SG, which demonstrated a sharper decrease in the stress level in EB. This decrease was even sharper for GB since the stress in GB-FPL was roughly 1.5 times higher than that in GS-FPL. However, due to the sharp decrease in the stress in GB, the stress level in GB-SG was 1.5 times lower than in GS-SG.

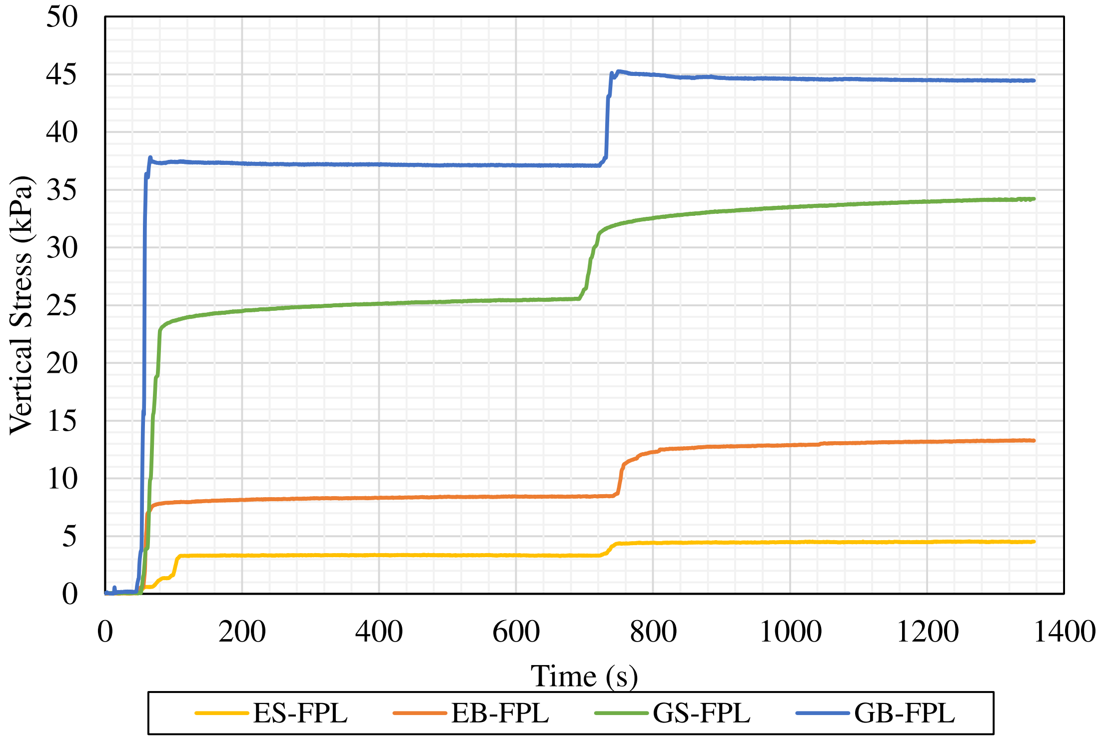

Figure 15: Vertical stresses in the FPL of all four tracks under static loading

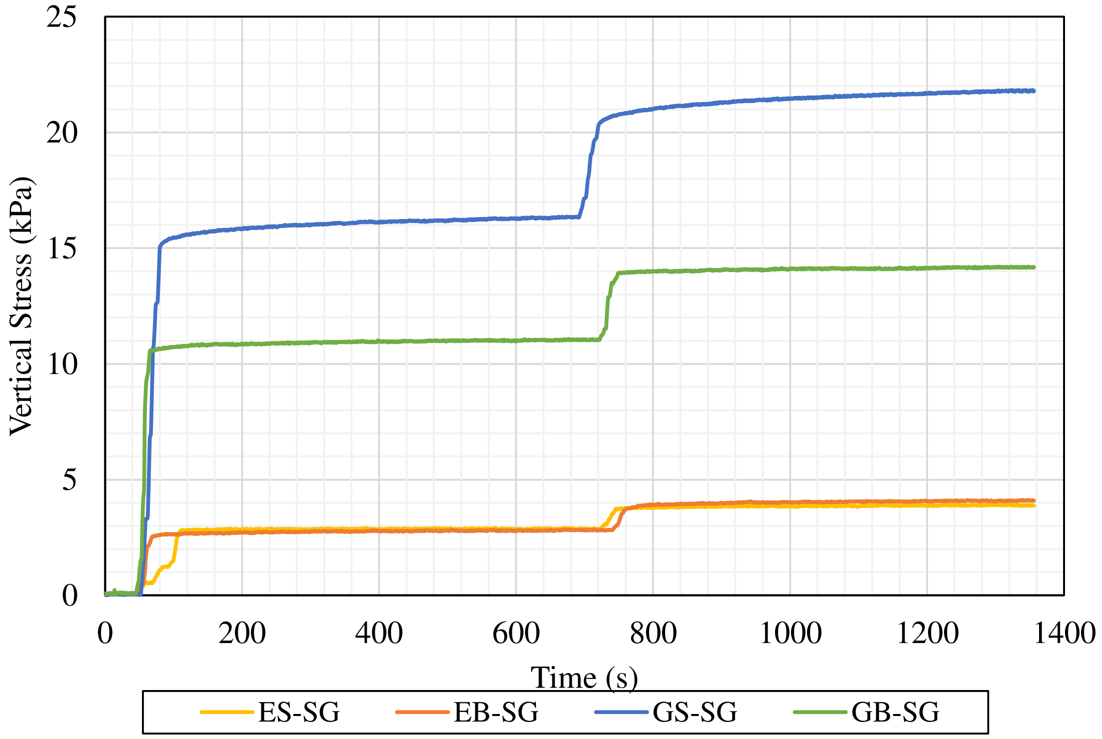

Figure 16: Vertical stresses in the subgrade of all four tracks under static loading

The continuous increase in the stress during the static loading in GS was because the GRS-RW was loaded for the first time and so residual settlement was important. The stresses in GB did not show the increase seen in GS as the GRS-RW structure was subjected to static and cyclic loading. GS testing led to a more settled and stiffer substructure for GB. The stress levels in the ES were 7 and 5 times less than the stresses in GS in the FPL and subgrade, respectively. They were 3.5 smaller in EB compared to GB. This is because of the GRS structure inducing more focused stresses in the central zone due to lower stress spread angle. ***Figure 17*** shows the stresses acting on the retaining wall of GRS-RW. The positive stress values were recorded for the ballasted track; however, they are negligibly small for this particular GRS type. The readings for GS were in the pressure cells margin of error that allows us to conclude there was no significant stress level on the wall.

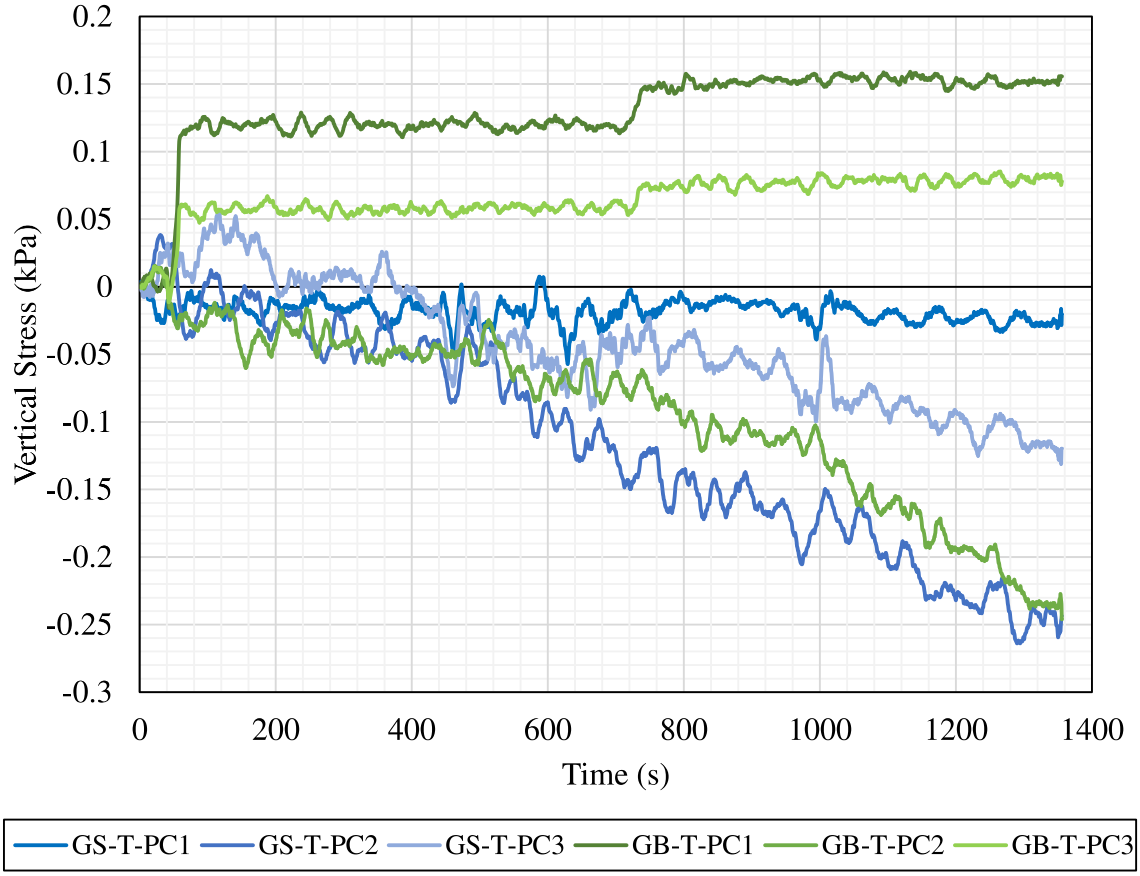

Figure 17: Vertical stresses on the retaining wall for the slab (GS) and the ballast (GB) tracks on the GRS-RW structure under static loading

The pressure readings on the wall, under both static and cyclic loadings, were negligibly small for these testing conditions. The pressure cells were calibrated prior to testing and it was confirmed that the cells were working properly. The GRS structure had expanded outwards under the action of compaction and reached its active state The pressure readings were lower than expected and hence this proves that the GRS structure worked as intended. The low pressure readings on the wall were also confirmed by ***Figure 7(d)***, which indicates no observable movement in the silicone sealent after the static and cyclic loadings.

4.2 Cyclic loading

In a stable track system, the magnitude and the number of axle loads are the key external factors for the permanent vertical track settlement. The differential permanent settlements cause uneven track geometry. The transient displacement under individual axles is an important component of the track behaviour. In a ballasted track, for example, if the track stiffness is too low then increased settlement is likely to occur, if it is too high then increased rail wear is likely to occur as a result. The elasticity of each layer contributes to the transient displacement. In addition to the elastic behaviour of the ballast, other physical parameters such as unbound nature of ballast, aggregate angularity and density are other reasons for larger displacements of ballasted tracks. Therefore, key parameters of permanent and transient displacement need to be identified by analysing the track behaviour under individual cycle as well as total cycles. The cycles, sinusoidal displacements, from beginning and end of the tests were recorded to calculate the stiffness change over the course of the cyclic loading. The cycles occurring per second were considered for Cyclic-1 and cyclic-2 tests. Four different LVDTs on Sleeper 1 and 3 were used to plot mean sinusoidal waves

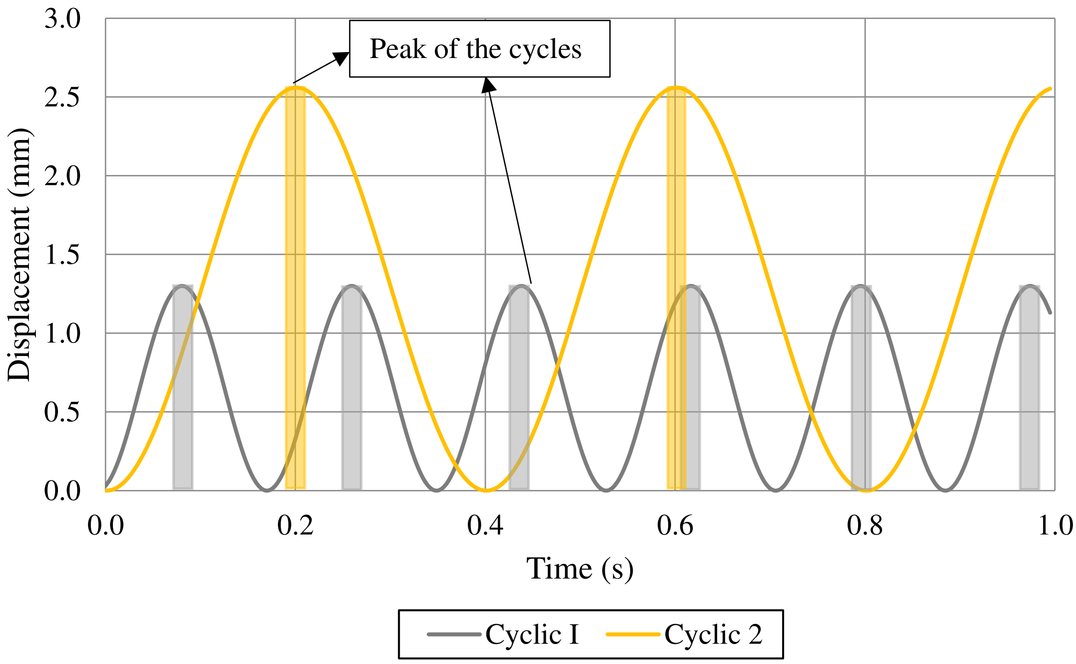

Figure 18: The use of bars corresponding to the peak of sinusoidal cycles

In this section, bar charts are employed to represent the data for clarity. The relative peak points of cycles were recorded to determine the amplitude of the sinusoidal cyclic motion. Then the amplitudes are presented as bars as shown in ***Figure 18***.

4.3 Rail and sleeper displacements

The rail deflections were obtained on the six LVDTs placed on the rails of the sleepers 1, 2 and 3. The deflections of the sleepers of the slab and ballasted tracks were obtained using the records of the four LVDTs placed on sleepers 1 and 3 i.e., at the corners of the track. The smoothness of the cycles is directly linked to the performance of the data acquisition system. However, instead of plotting sinusoidal curves under cyclic loading, bar charts are used to present the maximum relative displacements. The amplitudes are determined by taking 1000 cycles from the beginning of the tests and 1000 cycles before the end. The difference between the transient deflections under single cycles at the beginning and end of the loading can be neglected since it is in the margin of errors of the sensors. The figures below represent the rail displacements and the average of the six rails for all four track types.

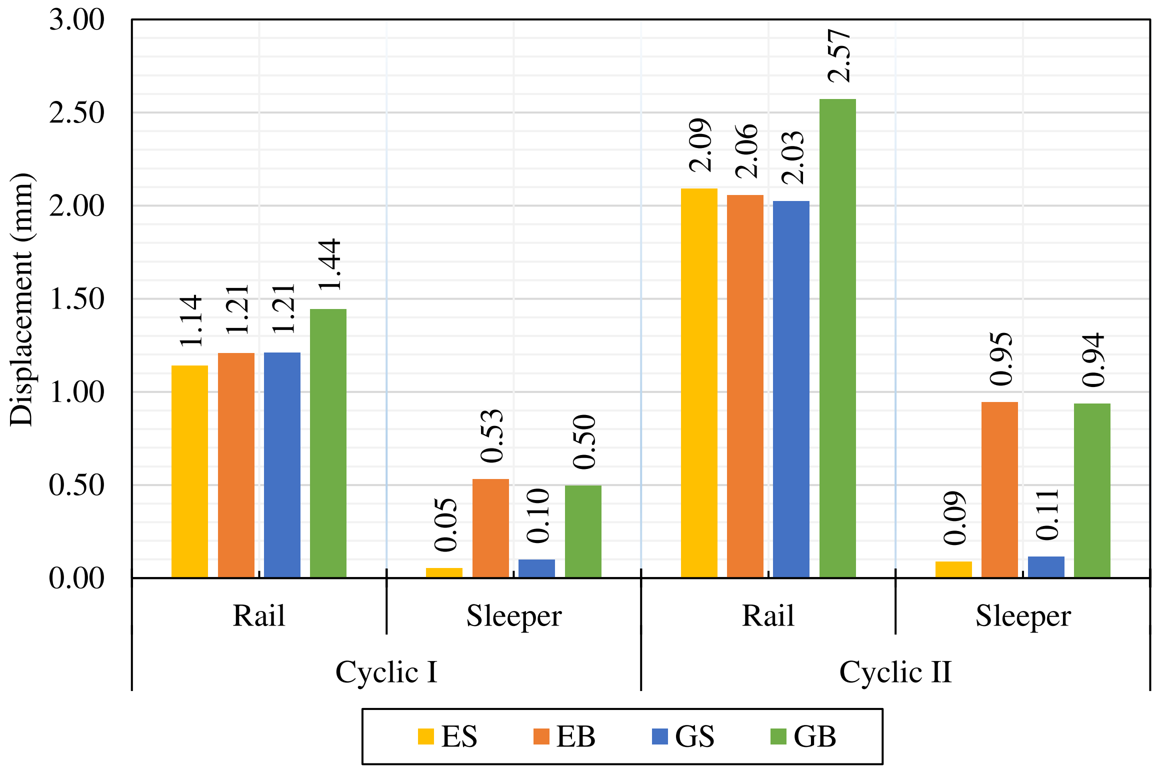

Figure 19: Average absolute displacements of the rails and sleepers (slab in the slab track case)

Figure 19 indicates the displacements of all rails and sleepers, for which the magnitude of the load on each actuator at 5.6Hz, 'Cyclic-I', was oscillating between 13kN and 58.9kN and for 2.5Hz, 'Cyclic-II', it was oscillating between 5kN and 83.4kN.

The displacement of the rails on the slab was 1.14mm and 1.21mm on the conventional embankment and GRS-RW structure, respectively, whereas it was 1.23mm and 1.46mm in the case of the ballasted track. Stiffening of the tracks due to shakedown was evident since all rail amplitudes decreased slightly through the end of the test. The reduction in the amplitude of the rail displacement was approximately 0.05mm for all tracks.

The rails on the slab deflected in a similar way on both substructures, whereas in the ballasted track case they deflected 2.57mm under the 83.4kN cyclic loading (as mentioned above which equates to a phased 17t axle load on individual sleepers without redistribution) on GRS-RW, which is 0.51mm larger than the deflection on the conventional embankment. The reduction in amplitude in the slab rails deflection was much smaller than that on the ballasted track.

Overall, the rails deflected with the largest values on ballasted track resting on GRS-RW structure (GB), as illustrated in ***Figure 19***. On the other hand, the displacements of the rails on the slab track placed on both substructures (ES-GS) and the ballasted track on the conventional embankment (EB) were very similar, while rails deflections on ES being slightly smaller than the rest. It is worth noting that the standard deviations of rail displacements on GRS-RW were smaller than those on the conventional embankment. GRS-RW provided the most uniform rail deflections and, in addition to that, the slab track exhibited the lowest standard deviation.

The slab track deflected 0.05mm and 0.1mm on ES and GS, respectively, whereas in the ballasted track case the deflection values were 0.53mm and 0.5mm on EB and GB, respectively at 'Cyclic-I'. The mean displacement of the slab under a single cycle for 'Cyclic-II' loading was 0.09mm in ES and 0.11mm in GS. The displacements of the sleepers in the ballasted track were 0.95mm and 0.94mm in EB and GB, respectively.

Contrary to the elastic behavior of the slab, ballast performed in a more complex manner due to its unbound and non-linear nature. While the deflection of the slab was quite uniform, according to the LVDTs on the slab, the deflection of the sleepers in the ballast varied among the LVDTs.

4.3.1 Pressure Cells

The maximum vertical peak stresses under Cyclic-I and Cyclic-II are presented in this section. The relative stresses were measured based on the cycles illustrated in ***Figure 9***. The loads exerted on the sleepers were oscillating between 30kN and 117.8kN for Cyclic-I, and between 9kN and 166.8kN for Cyclic-II. Therefore, the pressure cells always recorded positive values as there was always a force acting on the system. For this reason, relative magnitudes were plotted in ***Figure 20***, ***Figure 21*** and ***Figure 22*** rather than absolute values, which were used for LVDTs on rails and sleepers. It is notable that for Cyclic-I with 5.6Hz cyclic loading, the amplitudes of the stresses are significantly smaller than those at Cyclic-II with 2.5Hz cyclic loading.

The average stress under the ballast (EB) was 2.1 and 1.45 times higher than the stress under HBL (ES) at Cyclic-I and –II, respectively. Although the maximum stress was recorded in the centre of the middle sleeper in EB, the amplitudes were similar to each other for each cyclic test, whereas in ES, lower peaks and amplitudes were measured in the central pressure cell (***Figure 20***).

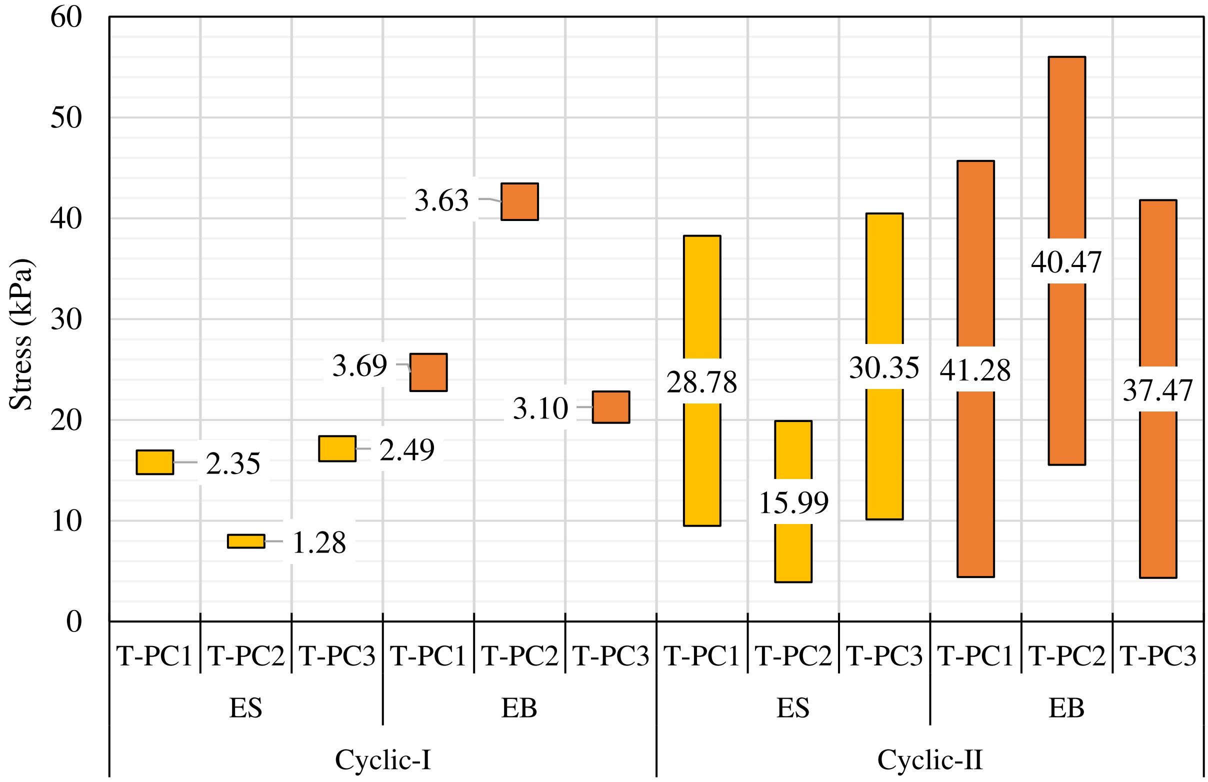

Figure 20: Relative stress amplitudes at the top of FPL in ballast and concrete slab track on the conventional embankment and GRS-RW structure at Cyclic-I and -II

The cyclic performance of the conventional embankment and GRS-RW was compared for FPL in ***Figure 21*** and the subgrade in ***Figure 22***. The peak stresses and amplitudes were lower deeper in the soil. In our experience, the pressure cells were not able to respond quickly enough to the change in pressure under the high frequency cyclic loading but, in the low frequency regime, they responded promptly. The highest-pressure levels were recorded in the subgrade and FPL of the GRS-RW track. The pressures were highly influenced by the boundaries of the tracks.

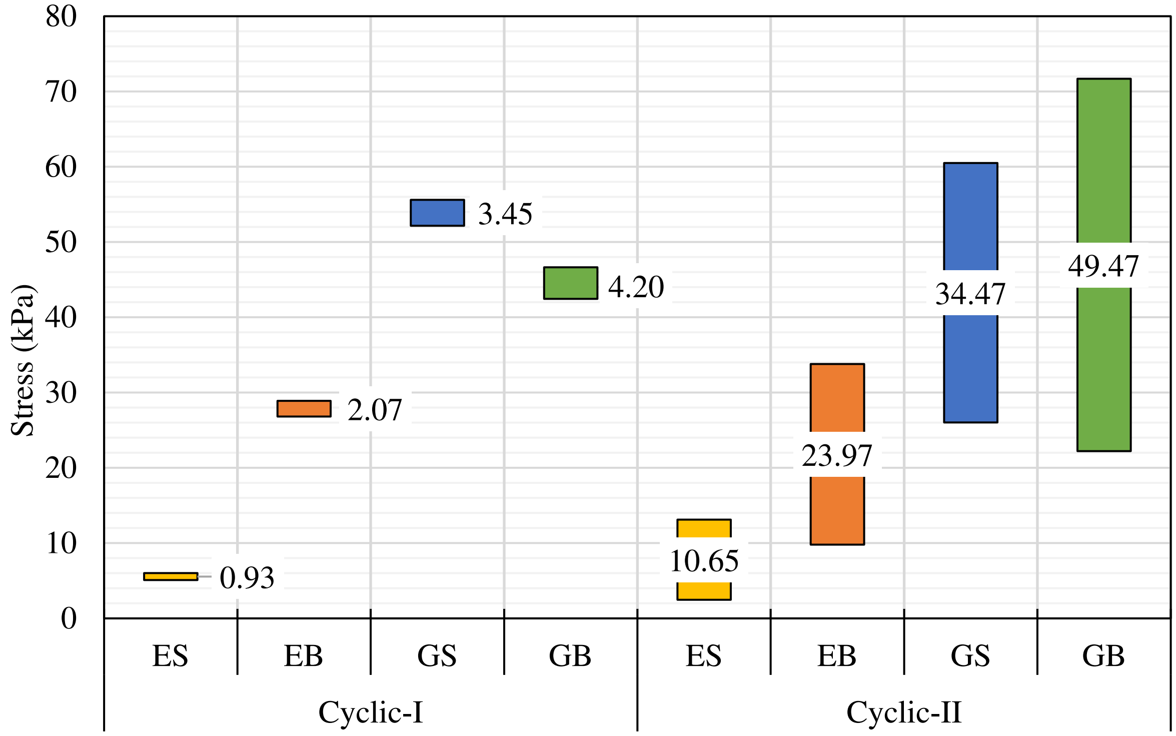

Figure 21: Relative stress amplitudes in FPL in ballast and concrete slab track on the conventional embankment and GRS-RW structure at Cyclic-I and -II

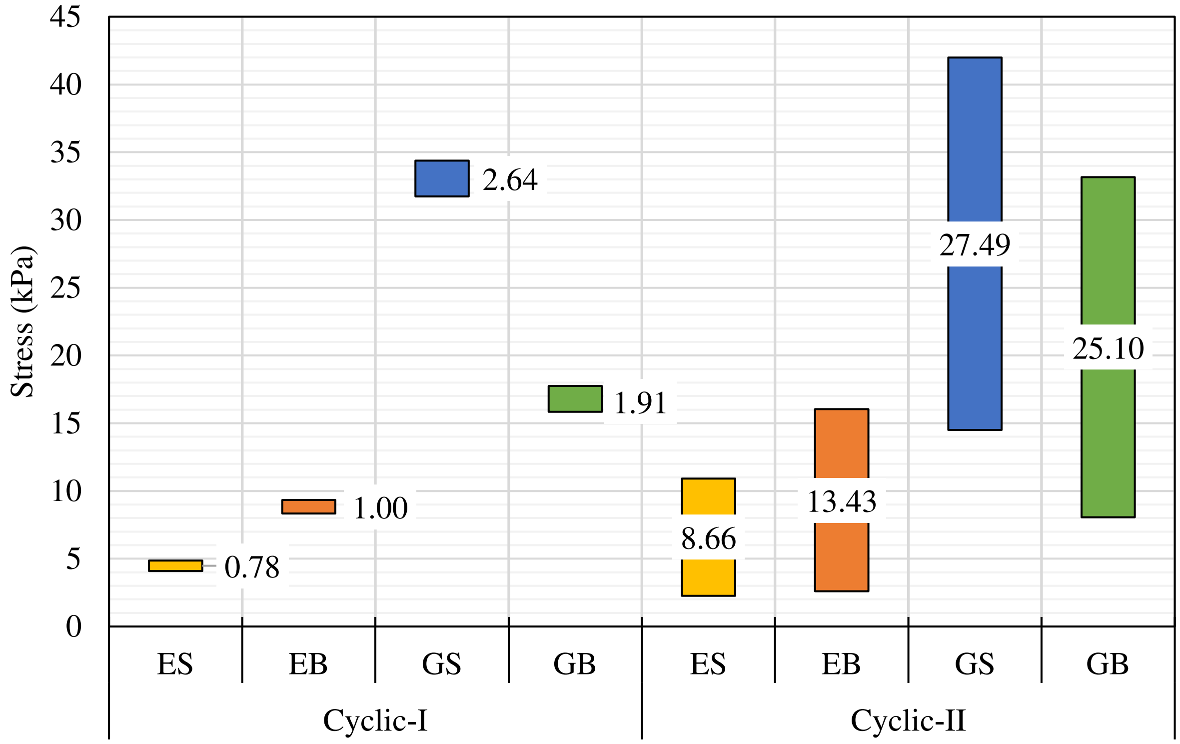

Figure 22: Relative stress amplitudes in subgrade in ballast and concrete slab track on the conventional embankment and GRS-RW structure at Cyclic-I and -II

4.3.2 Literature Comparison

The peak vertical stresses under static, cyclic and dynamic loadings were reported by various authors. Real dynamic field data measurements, full-scale laboratory testing and numerical analyses were conducted for ballasted, ballastless and trackbeds with hot mixed asphalt (HMA) railways. The stress values or range values obtained at the top surface of the FPL under different axle loads and speeds are presented with references in ***Table 4***.

Table 4: Stress measurements on top of the FPL (immediately under ballast/HBL) by various researchers

Reference	*Analysis type*	*Track Type*	*Axle Load (t)*	*Train Speed (km/h)*	*Stress (kPa)*
Liu and Xiao (2010)-I	Field	Ballast	22.50	120	29.9
Liu and Xiao (2010)-II	Field	Ballast	14.00	200	13.85
Bian et al (2014)-I	Field	Slab	14	330	14.6
Bian et al (2014)-II	Full scale test	Slab	14	330	15.9
Bian et al (2014)-III	Full scale test	Slab	17	5-360	18.2-19.6
Bian et al (2014)-IV	Full scale test	Slab	17	108-360	21.9-23.8
Indraratna et al (2010)- I	Field	Ballast	25	60	86.38
Indraratna et al (2010)- II	Field	Ballast	20.5	60	62.91
Xiaohong et al (2011)	Field	Slab	14	280-350	14.6-16.9
Hu and Li (2010)-I	Field	Slab	16	140-326	15-20
Hu and Li (2010)-II	Field	Slab	16	220-297	13-20
Dong et al (2008)	Field	Slab	14	45-160	10.2-17.6
Nie, et al (2005)	Field	Ballast	19.5	200-330	71.8-71.4
Hu and Li (2010)-III	Field	Ballast	22.5	10-400	70-100
Lamas-Lopez et al (2016)-I	Field	Ballast	22.5	60-200	13.0-14.2
Lamas-Lopez et al (2016)-II	Field	Ballast	10.5	60-200	8.2-9.7
Brown et al (2007)	Full scale test	Ballast	22.5	28	43-61
Zhang et al (2019)-I	Full scale test	Ballast	18	200	28.95
Zhang et al (2019)-II	Full scale test	Ballast	25	120	37.8
Li (2018)-I	Full scale test	Ballast	35.4	0	83
Li (2018)-II	Full scale test	HMA+Ballast	35.4	0	48-55
Li (2018)-III	Full scale test	Geocell+Ballast	35.4	0	65.5
Li (2018)-IV	Full scale test	HMA+Ballast	34.5	64	57.4
Jiang et al (2016)-I	3D FEM	Slab	14	360	15.6
Jiang et al (2016)-II	Field	Slab	14	270	19.5
Cardona et al (2014)-I	Field+2D FEM	Ballast	17	320	25.39
Cardona et al (2014)-II	2D FEM	GB+TS	17	320	15.16
Cardona et al (2014)-III	Field+ 2D FEM	GB	17	320	8.91
Rose et al (2004)-I	Field	HMA+Ballast	36	-	57.27
Rose et al (2004)-II	FEM-Kentrack	HMA+Ballast	36	-	55.2
Bian et al (2018)	Field+3D FEM	Slab	25	12.8-13.12	36-360

Grabe et al (2005)	Field+Geotrack	Ballast	26	47.5	100-108
Yang et al (2009)	2D FEM	Ballast	26	47.5	112-113
Domingo et al (2014)	3D FEM	Ballast	17	0	72.98
Slab-ST1-Fadum	Analytical	Slab	13	0	25.54
Slab-ST2- Fadum	Analytical	Slab	17	0	33.41
Ballast-ST1- Fadum	Analytical	Ballast	13	0	39.1
Ballast-ST2- Fadum	Analytical	Ballast	17	0	50.36

In addition to the measurements found in the literature, an analytical solution based on Fadum's chart [53] was considered for static loading to carry out a comparison with the outcomes of the presented experimental testing. The locations of the calculated stresses were the same as the depths of the pressure cells T-PC2, FPL-PC and SG-PC, with the depths being taken from the bottom of the ballast at 50mm, 200mm, and 800mm, respectively. The data collected in the current testing was used for comparison against the results found in the literature.

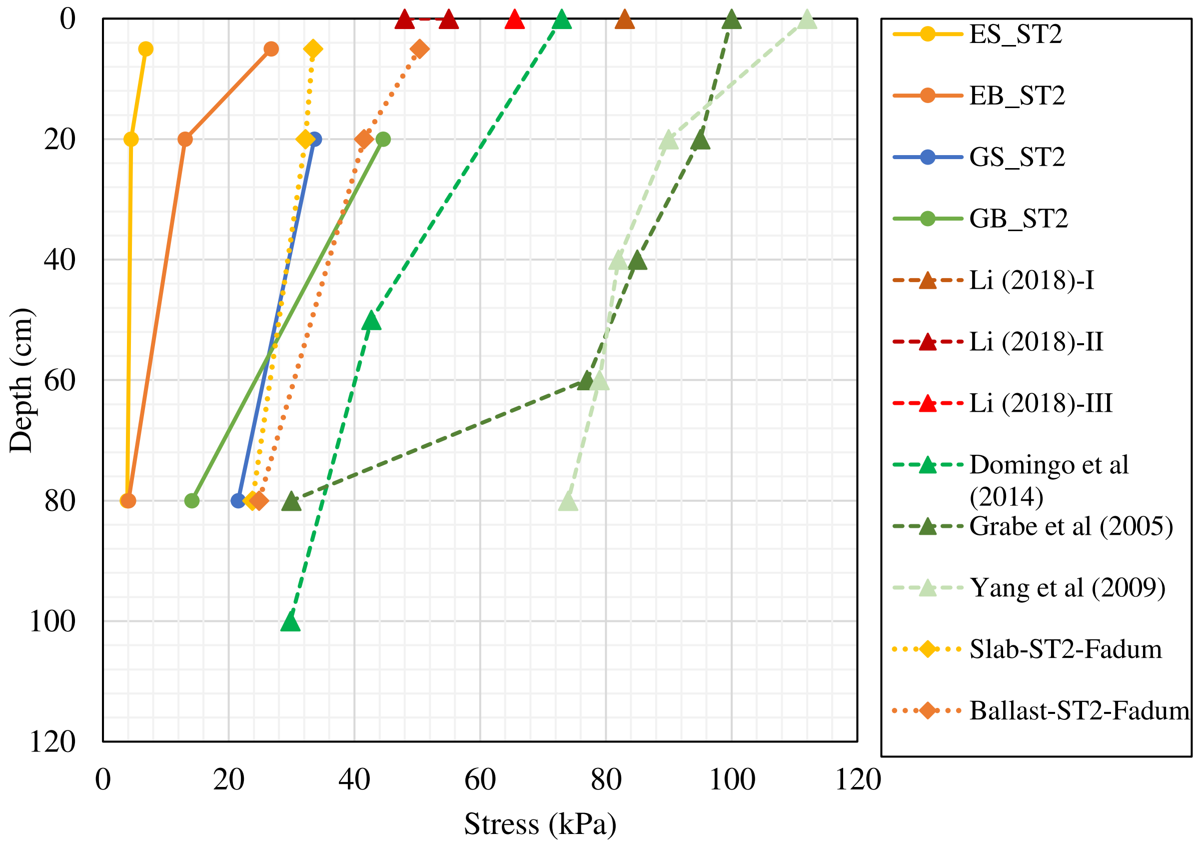

Figure 23: Absolute static stresses along depth from the surface of FPL

An empirical formula computing the vertical dynamic stress according to the Chinese high-speed railway code [61] is given as follows;

$$\sigma_{dmax} = 0.26P(1 + av)$$

where α is a speed coefficient, υ is the speed of the train and P is the axle load. As the stress value is linearly related to the axle load [61, 53], absolute stress measurements presented by other authors shown in ***Figure 23*** were recalculated for the value of 17t axle load for comparison purpose, as shown in **Figure 24**: **Relative static stresses along depth from the surface of FPL*Figure 24***.

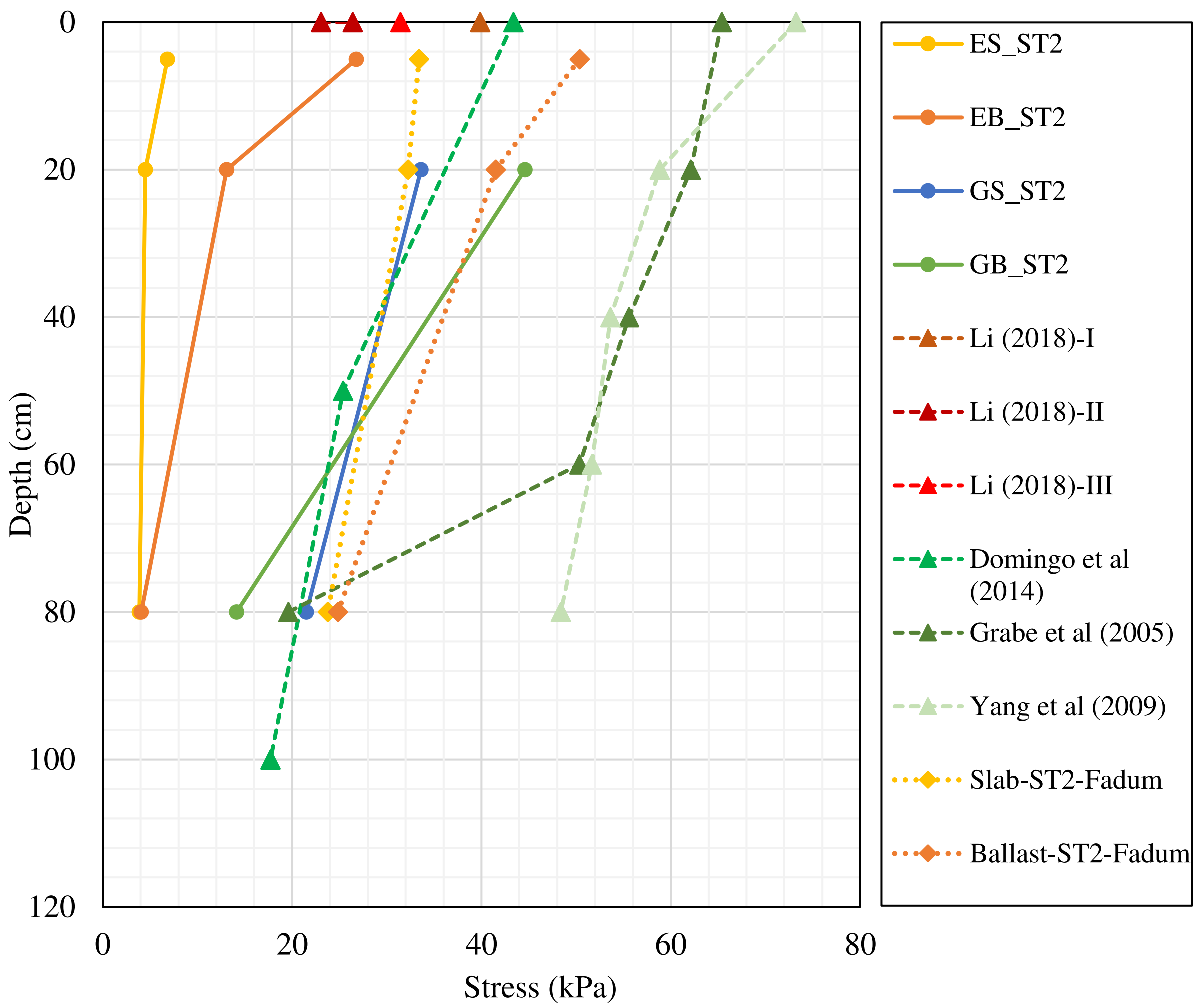

Figure 24: Relative static stresses along depth from the surface of FPL

The recalculated values represent the peak stresses along with the depth under static loading (Static-II). The stresses in ES and EB showed the lowest levels which are similar to the values presented by [25] in a trackbed with 200mm ballast and supported by 200mm thick HMA. Although the stresses in GS and GB were significantly higher than those in ES and EB, respectively, they matched well with the analytical results using Fadum's chart. Fadum's calculation assumes an infinitely large soil domain and does not take confinement into account. This proves the GRS-RW structure mimics well real rail track conditions as the lateral confinement is only provided by the geogrid and steel bars, whereas in the conventional embankment specimen, the lateral confinement was provided by the fixed metal walls.

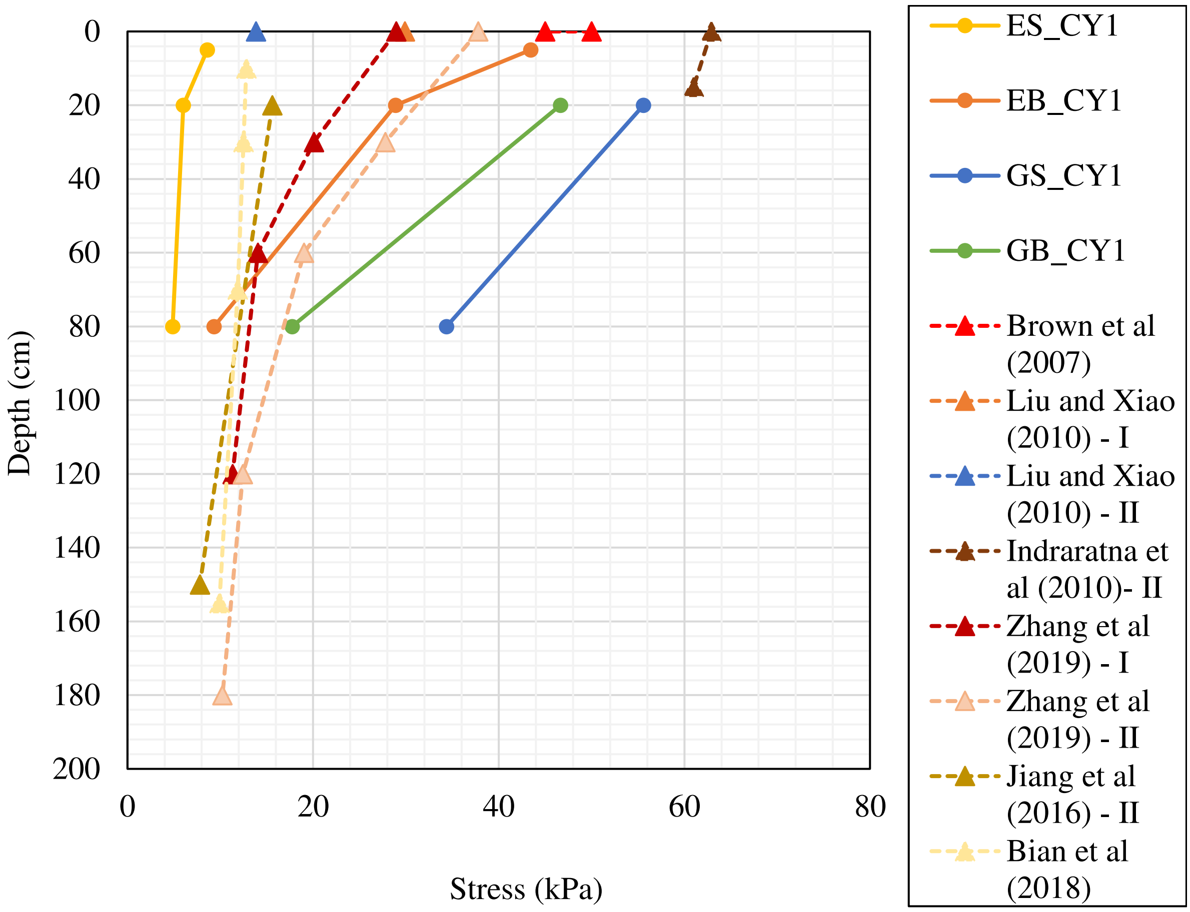

Figure 25: Comparison of vertical peak stresses from the FPL surface at Cyclic-I test (Estimated sleeper-ballast pressure 180-245kPa)

The absolute dynamic peak stresses under Cyclic-I loading at various locations beneath the track are presented in ***Figure 25*** . The stress value immediately under the middle sleeper was found to be 235kPa for Cyclic-I test. The stress values in the conventional embankment were smaller than those in the GRS-RW structure due to the lower deviatoric stresses. This is due to the lateral confinement provided by the fully fixed metal walls in the conventional embankment, whereas in the GRS-RW, the lateral confinement is provided by the geogrid reinforcement. The stress values decreased in the locations between 20cm and 80cm in the soil by 19% for ES, 68% for EB, 38% for GS and 62% for GB. The stress data collected for the ballasted track on the conventional embankment showed good agreement with that of the full-scale ballasted tests with similar axle load performed by Zhang *et al.* (2019)-1 [30].

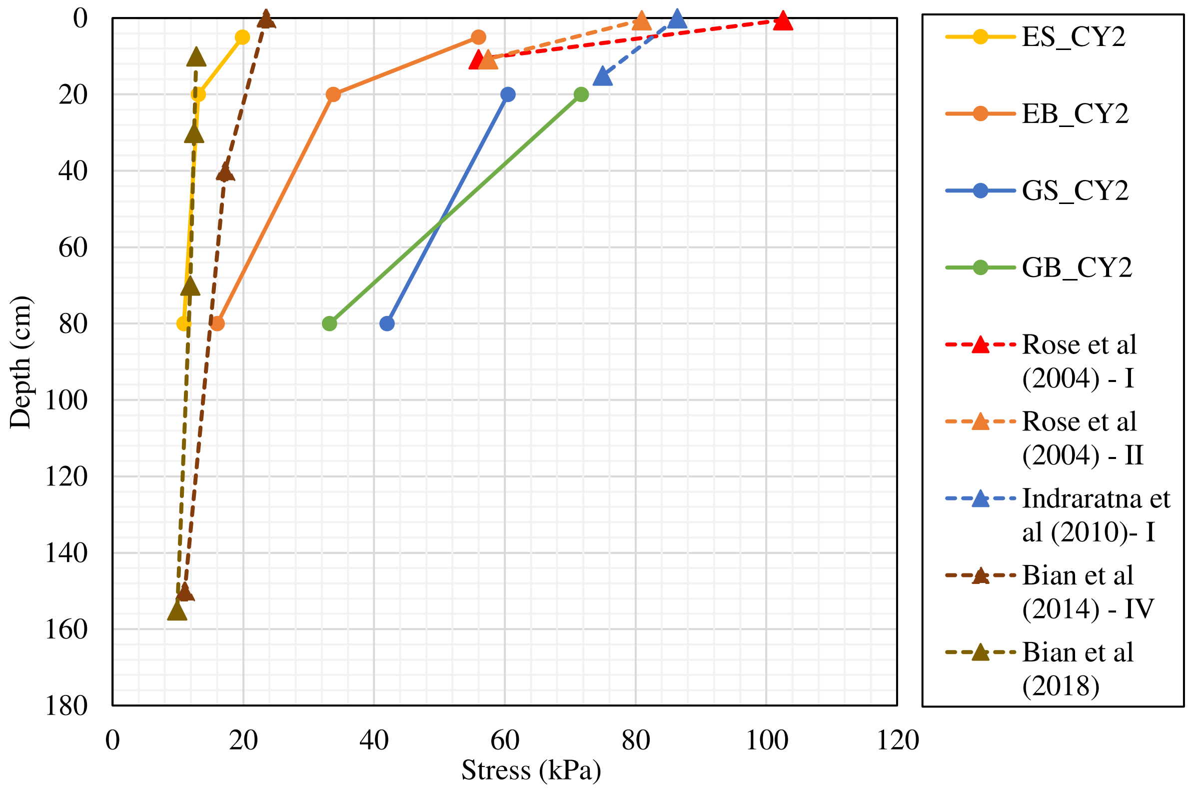

Figure 26: Comparison of vertical peak stresses from the FPL surface at Cyclic-II test (Estimated sleeper-ballast pressure 245-360kPa)

The stress under a sleeper during Cyclic-II testing was 333.5kPa. The measured stresses in the subgrade and the FPL show the values decreased by 17% for ES, 53% for EB, 31% for GS, and 54% for GB. The field data of a slab track resting on a conventional embankment collected by Bian *et al.* [40] had similar results as those of ES, which was subjected to similar axle loads ***Figure 26***.

5 Conclusions

A full-scale testing facility was used to identify the maximum vertical stresses in a low-level fully confined conventional embankment and a geosynthetically reinforced soil with retaining walls (GRS-RW). The transient displacements of the tracks and rails were obtained under two types of static and cyclic loadings. The phased manner of the actuators cyclic loading simulated the passage of a train traversing at 360km/h. The results were compared against published data, recorded during field measurements, full-scale laboratory testing, and numerical simulations carried and showed good agreement. The following conclusions were drawn:

- Although the stress levels in GRS-RW track were higher than in the conventional embankment, the decrease in stress with depth was greater. The stress on the wall under static and cyclic loading was negligibly small for these test setup conditions. This may not be the case for larger structures or more complex loading conditions.

- The pressure recordings on the GRS-RW wall were negligibly small as the readings were within the margin of the sensor errors. This proves that the GRS reached its active state and that the reinforced soil was already self-standing under its self-weight and train loads, therefore, there was practically no pressure on the walls. It was also observed during testing that the silicone sealant placed on the edges of the wall was intact after the tests, proving there are no observable movements of the walls.
- Overall, the stresses measured were consistent with other published works depending on the substructure. Based on the static and cyclic tests, the stress values in the soil of the GRS-RW structure were similar to field investigations performed by other researchers, and analytical solutions.
- The rails on slab tracks deflected similarly on both the conventional embankment and GRS-RW structure, while the rails on the ballasted track deflected 20% less on the conventional embankment compared to the ballasted track on GRS-RW. The sleeper displacements on the other hand were similar for the same type of superstructure.

Acknowledgements

The authors are grateful to the Engineering and Physical Sciences Research Council (EPSRC) for funding this work under Grant Number EP/N009207/1. Tarmac, Tensar and Max-Bőgl are also acknowledged for their support in supplying materials.

References

[1] J. T. Shahu and N. S. V. Kameswararao, "A rational method for design of railroad track foundation," *Soils and foundations,* vol. 40, no. 6, pp. 1-10, 2000.

[2] Z. Yu, P. Woodward, O. Laghrouche and D. Connolly, "True triaxial testing of geogrid for high speed railways," *Transportation Geotechnics,* p. 100247, 2019.

[3] R. Singh, S. Nimbalkar, S. Singh and D. Choudhury, "Field assessment of railway ballast degradation and mitigation using geotextile," *Geotextiles and Geomembranes,* vol. 48, no. 3, pp. 275-283, 2020.

[4] P. Punetha, S. Nimbalkar and H. Khabbaz, "Evaluation of additional confinement for three-dimensional geoinclusions under general stress state," *Canadian Geotechnical Journal,* vol. 57, no. 3, pp. 453-461, 2020.

[5] J. Koseki, R. J. Bathurst, E. Güler, J. Kuwano and M. Maugeri, "Seismic stability of reinforced soil walls," *Invited keynote paper, 8th International Conference of Geosynthetics, Yokohama,* pp. 18-22, 2006.

[6] F. Tatsuoka, M. Tateyama, Y. Mohri and K. Matsushima, "Remedial treatment of soil structures using geosynthetic-reinforcing technology," *Geotextiles and Geomembranes,* p. 204–220, 2007.

[7] J. Koseki, "Use of Geosynthetics to Improve Seismic Performance of Earth Structures," *Geotextiles and Geomembranes,* vol. 34, pp. 51-68, 2012.

[8] F. Tatsuoka, M. Tateyama, J. Koseki and T. Yonezawa, "Geosynthetic-Reinforced Soil Structures for Railways in Japan," *Transp. Infrastruct. Geotech,* p. 3–53, 2014.

[9] F. Tatsuoka and K. Watanabe, "Design, Construction, and Performance of GRS Structures for Railways in Japan," in *Ground Improvement Case Histories. Compaction, Grouting and*, Elsevier, 2015, pp. 657-692.

[10] M. Jia, W. Zhu and C. Xu, "Performance of a 33m high geogrid reinforced soil embankment without concrete panel," *Geotextiles and Geomembranes,* vol. 49, no. 1, pp. 122-129, 2021.

[11] U. Kim and D. Kim, "Load sharing characteristics of rigid facing walls with geogrid reinforced railway subgrade during and after construction," *Geotextiles and Geomembranes,* vol. 48, no. 6, pp. 940-949, 2020.

[12] J. Arivalagan, C. Rujikiatkamjorn, B. Indraratna and A. Warwick, "The role of geosynthetics in reducing the fluidisation potential of soft subgrade under cyclic loading," *Geotextiles and Geomembranes,* vol. 49, no. 5, pp. 1324-1338, 2021.

[13] S. Brown, B. Brodrick, N. Thom and G. McDowell, "The Nottingham railway test facility, UK," *Proceedings of the Institution of Civil Engineers-Transport,* vol. 160, no. 2, pp. 59-65, 2007.

[14] J. Liu and J. Xiao, "Experimental study on the stability of railroad silt subgrade with increasing train speed," *Journal of Geotechnical and Geoenvironmental Engineering,* vol. 136, no. 6, pp. 833-841, 2010.

[15] J. S. Anderson and J. G. Rose, "In-situ test measurement techniques within railway track structures," *ASME/IEEE Joint Rail Conference,* vol. 48124, pp. 187-207, 2008.

[16] J. G. Rose, D. B. Clarke, Q. Liu and a. T. J. Watts, "Application of Granular Material Pressure Cells to Measure Railroad Track Tie/Ballast Interfacial Pressures," *Transportation Research Record,* vol. 2672, no. 10, pp. 146-155, 2018.

[17] J. Rose, B. Su and F. Twehues, "Comparisons of railroad track and substructure computer model predictive stress values and in-situ stress measurements," Nashville, TN, September, 2004.

[18] B. Indraratna, S. Nimbalkar, D. Christie, C. Rujikiatkamjorn and J. Vinod, "Field assessment of the performance of a ballasted rail track with and without geosynthetics," *Journal of Geotechnical and Geoenvironmental Engineering,* vol. 136, no. 7, pp. 907-917, 2010.

[19] D. R. Cardona, H. D. Benedetto, C. Sauzeat, N. Calon and J. G. Rose, "Designs, Application and Performances of Asphalt/Bituminous Trackbeds in European, Asian, and African Countries," *Transportation Research Record,* p. 0361198120945314, 2020.

[20] L. Xiaohong, Y. Guolin and W. A. N. G. Liangliang, "Dynamic response testing and analysis on red-clay cutting bed under ballastless track of high-speed railway," *Geotechnical Investigation and Surveying,* vol. 39, no. 8, pp. 12-18, 2011.

[21] Y. F. Hu and N. F. Li, "Theory of ballastless track-subgrade for high speed railway," China Railway Published House, Beijing, 2010.

[22] L. Dong, C. Zhao, D. Z. Q. Cai and Y. Ye, "Experimental validation of a numerical model for prediction of the dynamic response of ballastless subgrade of high-speed railways," *China Civil Engineering Journal,* vol. 41, no. 10, pp. 81-86, 2008.

[23] Z. Nie, B. Ruan and L. Li, "Testing and analysis on dynamic performance of subgrade of Qinshen railway," *Journal of Vibration and Shock,* vol. 24, no. 2, pp. 30-32, 2005.

[24] F. Lamas-Lopez, Y.-J. Cui, N. Calon, S. C. D'Aguiar, M. P. D. Oliveira and T. Zhang, "Track-bed mechanical behaviour under the impact of train at different speeds," *Soils and Foundations,* vol. 56, no. 4, pp. 627-639, 2016.

[25] D. Li, "25 years of heavy axle load railway subgrade research at the Facility for Accelerated Service Testing (FAST)," *Transportation Geotechnics,* vol. 17, pp. 51-60, 2018.

[26] E. Selig and D. Li, "Track modulus: Its meaning and factors influencing it," *Transportation Research Record,* no. 1470, p. 47–54, 1994.

[27] Z. Yu, D. P. Connolly, P. K. Woodward and O. Laghrouche, "Settlement behaviour of hybrid asphalt-ballast railway tracks," *Construction and Building Materials,* vol. 208, pp. 808-817, 2019.

[28] H. Jiang, X. Bian, C. Cheng, Y. Chen and R. Chen, "Simulating train moving loads in physical model testing of railway infrastructure and its numerical calibration," *Acta Geotechnica,* vol. 11, no. 2, pp. 231-242, 2016.

[29] R. Chen, X. Zhao, Z. Wang, H. Jiang and X. Bian, "Experimental study on dynamic load magnification factor for ballastless track-subgrade of high-speed railway," *Journal of Rock Mechanics and Geotechnical Engineering,* vol. 5, no. 4, pp. 306-311, 2013.

[30] C. Zhang, G. Jiang, O. Buzzi and L. Su, "Full-scale model testing on the dynamic behaviour of weathered red mudstone subgrade under railway cyclic loading," *Soils and Foundations,* vol. 59, no. 2, pp. 296-315, 2019.

[31] S.-H. Lee, K.-Y. Eum, T. H. M. Le and D.-W. Park, "Evaluation on mechanical behavior of asphalt concrete trackbed with slab panel using full-scale static and dynamic load test," *Construction and Building Materials,* vol. 276, p. 122207, 2021.

[32] M. P. Sysyn, V. V. Kovalchuk, O. S. Nabochenko, Y. Kovalchuk and O. M. Voznyak, "Experimental Study of Railway Trackred Pressure Distribution under Dynamic Loading," *The Baltic Journal of Road and Bridge Engineering,* vol. 14, no. 4, pp. 504-520, 2019.

[33] J. Rose, M. L. Purcell and Q. Liu, "Suitability of Earth and Granular Materials Pressure Cells for Measuring Railway Trackbed Tie/Ballast Interfacial Pressures," *In ASME/IEEE Joint Rail Conference, vol. 49675, p. V001T01A010. American Society of Mechanical Engineers,* 2016.

[34] G. A. Miller, S. Y. Teh, D. Li and M. M. Zaman, "Cyclic shear strength of soft railroad subgrade," *Journal of Geotechnical and Geoenvironmental Engineering,* vol. 126, no. 2, pp. 139-147, 2000.

[35] D. Li and E. T. Selig, "Resilient modulus for fine-grained subgrade soils," *J. Geotech. Engrg., ASCE,* vol. 120, no. 6, p. 939–957, 1994.

[36] Z. Yu, D. Connolly, P. Woodward, O. Laghrouche and E. Tutumluer, "Railway ballast anisotropy testing via true triaxial apparatus," *Transportation Geotechnics,* vol. 23, p. 100355, 2020.

[37] Y. Momoya, E. Sekine and F. Tatsuoka, "Deformation characteristics of railway roadbed and subgrade under moving-wheel load," *Soils and Foundations,* vol. 45, no. 4, pp. 99-118, 2005.

[38] T. Ishikawa, E. Sekine and S. Miura, "Cyclic deformation of granular material subjected to moving-wheel loads," *Canadian Geotechnical Journal,* vol. 48, no. 5, pp. 691-703, 2011.

[39] X. Bian, H. Jiang, C. Cheng, Y. Chen, R. Chen and J. Jiang, "Full-scale model testing on a ballastless high-speed railway under simulated train moving loads," *Soil Dynamics and Earthquake Engineering,* vol. 66, pp. 368-384, 2014.

[40] X. Bian, W. Li, J. Hu, H. Liu, X. Duan and Y. Chen., "Geodynamics of high-speed railway," *Transportation Geotechnics,* vol. 17, pp. 69-76, 2018.

[41] L. A. Yang, W. Powrie and J. A. Priest, "Dynamic stress analysis of a ballasted railway track bed during train passage," *Journal of Geotechnical and Geoenvironmental Engineering,* vol. 135, no. 5, pp. 680-689, 2009.

[42] W. Powrie, L. Yang and C. Clayton, "Stress changes in the ground below ballasted railway track during train passage," *Proceedings of the Institution of Mechanical Engineers, Part F: Journal of Rail and Rapid Transit,* vol. 221, no. 2, pp. 247-262, 2007.

[43] P. J. Grabe, C. R. I. Clayton and F. J. Shaw, "Deformation measurement on a heavy haul track formation," Rio de Janeiro, Brazi, 2005.

[44] D. R. Cardona, J. Benkahla, S. C. D'Aguiar, N. Calon, A. Robinet, H. D. Benedetto and C. Sauzeat, "High-speed ballasted track behavior with sub-ballast bituminous layer," in *Proceedings of the 2nd international symposium on railway geotechnical engineering*, Marne-la-Vallée, France, 2014.

[45] D. R. Cardona, H. D. Benedetto, C. Sauzeat, N. Calon and G. Saussine, "Use of a bituminous mixture layer in high-speed line trackbeds," *Construction and Building Materials,* vol. 125, pp. 398-407, 2016.

[46] L. M. Domingo, C. Z. Martín, C. P. Avilés and J. I. R. Herráiz, "Analysis of the influence of cracked sleepers under static loading on ballasted railway tracks," *The Scientific World Journal,* 2014.

[47] ORE, "Question D117: Optimum adoption of the conventional track to future traffic. Report No. 28: Design charts for the track/foundation system, " Report D117/RP 28"," ORE, Utrecht, Netherlands, 1983.

[48] Y. Shan, S. Zhou, B. Wang and C. L. & Ho, "Differential Settlement Prediction of Ballasted Tracks in Bridge–Embankment Transition Zones," *Journal of Geotechnical and Geoenvironmental Engineering,* vol. 146, no. 9, p. 04020075, 2020.

[49] K. Dong, D. Connolly, O. Laghrouche, P. Woodward and P. Costa, "The stiffening of soft soils on railway lines," *Transportation Geotechnics,* vol. 17, pp. 178-191, 2018.

[50] K. Dong, D. Connolly, O. Laghrouche, P. Woodward and P. Costa, "Non-linear soil behaviour on high speed rail lines," *Computers and Geotechnics,* vol. 112, pp. 302-318, 2019.

[51] A. Ramos, A. Correia, R. Calçada, P. Costa, A. Esen, P. Woodward, D. Connolly and O. Laghrouche, "Influence of track foundation on the performance of ballast and concrete slab tracks under cyclic loading: Physical modelling and numerical model calibration," *Construction and Building Materials,* vol. 277, p. 122245, 2021.

[52] L. Bathurst and A. Kerr, "An improved analysis for the determination of required ballast depth," *Proceedings AREMA on Track and Struct,* pp. 916-947, 1999.

[53] R. E. Fadum, "Influence values for estimating stresses in elastic foundations," *Proc. 2nd Int. Conf. Soil Mechanics and Foundation Engineering,* vol. 3, pp. 77-84, 1948.

[54] T. M. Čebašek, A. F. Esen, P. K. L. O. Woodward and D. P. Connolly, "Full scale laboratory testing of ballast and concrete slab tracks under phased cyclic loading," *Transportation Geotechnics,* vol. 17, pp. 33-40, 2018.

[55] A. Esen, P. Woodward, O. Laghrouche, T. M. Čebašek, A. Brennan, S. Robinson and D. Connolly, "Full-Scale Laboratory Testing of a Geosynthetically Reinforced Soil Railway Structure," *Transportation Geotechnics,* vol. 28, p. 100526, 2021.

[56] B. 1377-4-1990, "BS 1377-4-1990, Methods of test for Soils for civil engineering purposes-Part4: Compaction-related tests," British Standard institute, London: UK, 1990.

[57] TRRL Road Note 8, "A users manual for a program to analyse dynamic cone penetrometer data," Transport and Road Research Laboratory, Crowthorne Berkshire United Kingdom, 1990.

[58] DIN:18134, "Determining the deformation and strength characteristics of soil by the plate loading test," 2001.

[59] B. Lichtberger, Track Compendium, 2005, pp. 1-192.

[60] J. Koseki, Use of Geosynthetics to Improve Seismic Performance of Earth Structures, http://www.mercerlecture.com/, 2009.

[61] TB10621, "Ministry of Railways of People's Republic of China, Code for design of high speed railway," China Railway Press, Beijing, China, 2009.

[62] T. Wang, Q. Luo, L. Zhang and J. Yao, "Dynamic response of subgrade in a bridge transition along the Qinhuangdao-Shenyang high-speed rai".

[63] X. Bian, H. Jiang, Y. Chen, J. Jiang and J. Han, " A full-scale physical model test apparatus for investigating the dynamic performance of the slab track system of a high-speed railway," *Proceedings of the Institution of Mechanical Engineers, Part F: Journal of Rail and Rapid Transit,* vol. 230, no. 2, pp. 554-571, 2016.

[64] K. Horii, H. Kishida, M. Tateyama and F. Tatsuoka, "Computerized design method for geosynthetic-reinforced soil retaining walls for railway embankments. Recent Case Histories of Permanent Geosynthetic-Reinforced Soil Retaining Walls," *ecent Case Histories of Permanent Geosynthetic-Reinforced Soil Retaining Walls,* pp. 205-218, 1994.

[65] J. Koseki, Y. Munaf, F. Tatsuoka, M. Tateyama, K. Kojima and T. Sato, "Shaking and tilt table tests of geosynthetic-reinforced soil and conventional-type retaining walls.," *Geosynthetics international,* pp. 73-96, 1996.

[66] F. Tatsuoka, M. Tateyama, T. Uchimura and J. Koseki, "Geosynthetic-reinforced soil retaining walls as important permanent structures Geosynthetics international," *Geosynthetics international, Vol. 4, No. 2,* pp. 81-135, 1997.

[67] T. Yonezawa, T. Yamazaki, M. Tateyama and F. Tatsuoka, "Design and construction of geosynthetic-reinforced soil structures for Hokkaido high-speed train line," *Transportation Geotechnics,* pp. 3-20, 2014.

[68] F. Tatsuoka, "Geosynthetic-reinforced soil structures for transportation: from walls to bridges," in *Australia New Zealand Conference on Geomechanics, 13th, 2019, Perth, Western Australia*, Australia, 2019.

[69] ISO, SIST-TS CEN., ""TS 17892-4: 2004: Geotechnical Investigation and Testing–Laboratory Testing of Soil–Part 4: Determination of Particle Size Distribution (ISO/TS 17892-4: 2004)," Inštitut za standardizacijo, Slovenija, 2004.